UC Riverside

UC Riverside Electronic Theses and Dissertations

Title

Studies of Various Hydrocarbon Conversion Reactions on Pt Catalysts

Permalink

https://escholarship.org/uc/item/74p2788m

Author

Kaneko, Shinji

Publication Date

2011

Peer reviewed|Thesis/dissertation

eScholarship.org Powered by the California Digital Library
University of California

UNIVERSITY OF CALIFORNIA
RIVERSIDE

Studies of Various Hydrocarbon Conversion Reactions on Pt Catalysts

A Thesis submitted in partial satisfaction
of the requirements for the degree of

Master of Science

in

Chemistry

by

Shinji Kaneko

December 2011

Thesis Committee:

Prof. Francisco Zaera, Chairperson

Prof. David F. Bocian

Prof. Christopher J. Bardeen

Copyright by
Shinji Kaneko
2011

The Thesis of Shinji Kaneko is approved:

Committee Chairperson

University of California, Riverside

Acknowledgement

First of all, I am very grateful with Professor Francisco Zaera for having giving me the opportunity, guidance and assistance throughout my graduate studies. His valuable comments and discussions about my research gave me an idea of what might be the next step to continue with my work.

I would like to thank Professors Janet Aray, Yadong Yin, and Krassimir Bozhilov for the help with gas chromatography, colloidal nanoparticle preparation, and transmission electron microscopy. I am thankful to Professors David Bocian, Christopher Bardeen, Pingyun Feng, and Yushan Yan for being the committee for this dissertation, and Professor Ryan Julian as graduate advisor. Dr. Richard Kondrat, Stephan McDaniel, Kris Pranata, Aiko Matsunaga, Qiao Zhang helped me with GC-MS, TEM, UV-Vis, gas chromatography, and colloidal nanoparticle preparation, respectively. I also appreciate all the help provided by department staff members, Linda Edwards, Barbara Outzen, Tina Enriquez, Wayne Kaylor, Priscilliano Saavedra, Colleen Fleming, Micheal Fournier, Jeff Lefler, and Christina Youhas.

I am also grateful to my labmates: Dr. Ilkeun Lee, for being able to help me and guide me with all the experiments I conducted; Stan Sheldon, for his help in the electronic and glass instruments; Dr. Ricardo Morales, for helping me learn how to use UHV chamber; Dr. Aashani Tillekarante, for many proofreading and advise; Dr. Min Shen, Dr. Qiang Ma, Dr. Xiandong Qin, Dr. Taeseung Kim, Dr. Maryam Ebrahimi, Dr. Ji Bong Joo, Dr. Lenxia Cheng, Dr. Zhihuang Weng, Dr. Karakalos Stavros Georgios, Dr. Golam Moula, Menno Bouman, Junghyn Hong, Hoaxing Sun, Xin Yang, Yang Li, Lei Guo, Timothy, Renee, Ryan Pedigo, Bunn Chinkulkitnivat, Chris,

Svetlana Borukhova, Xiao Xiao, Christopher Clark, for their friendship and help. I learned something valuable from all of you.

I would also thank all my friends I met on and off campus during my graduate study. I had a good time thanks to all of you.

Last, but no least, I am thankful to the support that was given from my family.

Table of contents

Chapter 1: Introduction…….……,,……..1

Chapter 2: Chiral catalysis – adsorption of 1-(1-naphthyl)ethylamine on Pt(111) surface……..2

2.1. Introduction…….,……2

2.2. Experimental…….....6

2.3. Results……...8

2.4. Conclusions…….20

2.5. References……...21

Chapter 3: Hydrogenation reactions on shape controlled catalysts……22

3.1. Introduction...……...…….....22

3.2. Experimental……...……29

3.2.1. Preparation of catalysts…….……...……...29

3.2.1.1. Preparation of normal Pt/SiO_2 catalysts…….……..……..29

3.2.1.2. Preparation of colloidal tetrahedral particles……..…….....……..30

3.2.1.3. Preparation of colloidal cubic particles…….…..……..……..30

3.2.1.4. Deposition of colloidal particles on SiO_2 xerogel……..…..……..30

3.2.2. TEM measurements……..……..……..……..30

3.2.3. Gas-phase circulation reaction…….……..……..……..31

3.2.3.1. Hydrogenation of crotonaldehyde.…….……..……..33

3.2.3.2. Hydrogenation of isoprene……...……..……..…..……..33

3.2.3.2. Hydrogenation of other reactant..……..……...……..……..33

3.3. Results…….35

3.3.1. Hydrogenation of crotonaldehyde……...……..……..……...35

3.3.1.1. Prepared catalysts……..……...…….……..……..35

3.3.1.2. Hydrogenation……...……....……..……..35

3.3.2. Other hydrogenation reactions…..…….....……..……..41

3.3.3. Hydrogenation of isoprene……...……..……..……..43

3.3.3.1. Preliminary result……..……...…….……..……..43

3.3.3.2. Reproducibility improvement…...…….……..……..43

3.3.3.3. Reaction without silanized wool and coarse wool…....……..45

3.3.3.4. Preparation of tetrahedral catalysts…...…..…..……..……..50

3.3.3.5. Preparation of cubic catalysts…...…….……..……..50

3.3.3.6. Comparison of catalysts…...……..……..…….……..……..53

3.4. Conclusions…...……..……..……..……...……..60

3.5. References…...……..……...……61

Chapter 4: Conclusions……...……62

List of Figures

Figure 2.1. Chemical structures……4

Figure 2.2. RAIRS for (*R*)-NEA adsorbed on a single-crystal Pt(111) surface at 80 K under UHV as a function of initial exposure……..9

Figure 2.3. PO-titration TPD traces from Pt(111) surfaces first dosed with various amounts of (*R*)-NEA and then with 2.0 L of (*R*)- PO at liquid nitrogen temperatures…….11

Figure 2.4. PO-titration TPD traces from Pt(111) surfaces first dosed with various amounts of (*R*)-NEA and then with 2.0 L of (*S*)- PO at liquid nitrogen temperatures…….12

Figure 2.5. An example of deconvolution result (1.0 L of (R)-NEA and 2.0 L of R-PO)……..13

Figure 2.6. Monolayer PO desorption yields, estimated from the TPD titration experiments in Figure 2.8 and 2.9, as a function of initial (*R*)-NEA exposure……..16

Figure 2.7. RAIRS from Pt(111) surfaces first exposed to various amounts of (*R*)-NEA and then to 1.0 L of (*S*)- or (*R*)-PO……...17

Figure 2.14. Details of the RAIRS data in Figure 2.11, highlighting the signals from the ring-deformation mode of PO……18

Figure 3.1. Hydrogenation of isoprene……...24

Figure 3.2. Reported reaction result of isoprene hydrogenation on Pt(111)……...25

Figure 3.3. Expected adsorbed surface species into partial hydrogenation products……..…...26

Figure 3.4. Hydrogenation of crotonaldehyde……..…..28

Figure 3.5. Gas-phase circulation reactor……..…….32

Figure 3.6. TEM image of 0.5 wt% normal Pt/SiO_2 calcined at 300 °C……..36

Figure 3.7. TEM image of 0.5 wt% normal Pt/SiO_2 calcined at 500 °C……...37

Figure 3.8. TEM image of 0.5 wt% normal Pt/SiO_2 calcined at 700 °C……...38

Figure 3.9. TEM image of colloidal tetrahedral particles prepared by Dr. Ilkeun Lee…….39

Figure 3.10. TEM image of 0.5 wt% supported tetrahedral Pt/SiO_2 prepared by Dr. Ilkeun Lee..40

Figure 3.11. Isoprene hydrogenation on 0.5 wt% normal and tetrahedral Pt/SiO_2 (preliminary result)…….44

Figure 3.12. Isoprene hydrogenation on normal Pt/SiO_2 with or without silanized wool……..46

Figure 3.13. Isoprene hydrogenation - effect of pretreatment with coarse wool……47

Figure 3.14. Isoprene hydrogenation - effect of pretreatment with coarse wool……48

Figure 3.15. Colloidal tetrahedral particles…….51

Figure 3.16. 0.5 wt% supported tetrahedral particles…….52

Figure 3.17. Colloidal cubic particles…….54

Figure 3.18. 0.5 wt% supported cubic particles……..55

Figure 3.19. Hydrogenation of isoprene on 0.5 wt% normal Pt/SiO_2…….56

Figure 3.20. Hydrogenation of isoprene on tetrahedral Pt/SiO_2…….57

Figure 3.21. Hydrogenation of isoprene on cubic Pt/SiO_2……..58

List of Tables

Table 2.1. Vibrational assignments of the peaks in the RAIRS data for pure NEA and for NEA adsorbed on platinum surfaces……10

Table 2.2. Deconvolution data of R/R pair……14

Table 2.3. Deconvolution data of S/S pair……14

Table 2.4. Area of monolayer desorption peak……..……14

Table 2.5. Deconvolution of ring deformation peak…..……19

Table 3.1. Hydrogenation of crotonaldehyde on normal- and tetra-Pt/SiO_2……..42

Chapter 1: Introduction

The basic concept of heterogeneous catalysis was built on the concept of catalysis proposed in the 1830s by Berzelius and Emmett. Catalysts are materials that facilitate chemical reactions without seemingly participating in these reactions. In the late 19th century, Ostwald proved that catalysts indeed accelerate reaction rates. The dispute between Nernst and Habor on ammonia synthesis did a great deal for the development of physical chemistry. In the late 1960s/early 1970s, Boudart classified catalytic reactions into two groups: structure sensitive and structure insensitive. The structure sensitive reaction changes their rate as a function of particle size, while structure insensitive reactions remain at a constant rate as the particle size increases. Over the last several decades, surface science has undergone revolutionary advances that reveal on the atomic- and molecular-level structural properties of surfaces.

I spent 5 years of my time for the research in the field of catalysis. My work on chiral catalysis project is described in chapter 2. In chapter 3, gas-phase hydrogenation reaction on shape controlled Pt catalysts was summarized.

Besides these two projects, I also worked on many other projects: investigation of crystal energy of cinchona alkaloids with bomb calorimetry and theoretical calculations, “high pressure” surface science study, cis-trans isomerization of 2-butenes, and liquid-phase hydrogenation reactions, although they are not included in this thesis.

Chapter 2: Chiral catalysis – Adsorption of 1-(1-Naphthyl)Ethylamine on Pt(111) Surface

2.1. Introduction

Development of enantioselective processes is desirable for the increasing prominence of chiral synthesis in the pharmaceutical and agro industries[1]. Especially the ones utilize heterogeneous catalysts are advantageous due to the ease of handling and separation compared to homogeneous systems that are common nowadays in many applications. Therefore the realization of heterogeneous system would make current industrial processes cheaper and greener. Unfortunately no viable heterogeneous enantioselective catalysts are available to date for practical use[2].

The use of chiral modifiers is one of the most viable approaches for enantioselective heterogeneous catalysis. The hydrogenation of β-ketoesters using tartaric acid-modified nickel catalysts[3] and the hydrogenation of α-ketoesters using platinum catalysts modified by cinchona alkaloids[4] are the two most well-known systems. There are a few variations of these reported, but their extensions to other more general systems have not yet been realized[5].

Importantly, these two known cases have been explained by significantly different mechanisms. Each individual molecule of cinchona alkaloids is believed to possess ability to impart chirality to catalytic reactions, possibly forming a complex with the reactant on the surface of the catalysts in such a way as to force specific adsorption geometry and leads to the selective hydrogenation[6]. On the other hand, tartaric acid is a much simpler molecule and may not be able to individually form a 1:1 complex. Instead, the formation of supramolecular chiral structures has

been suggested[7]. The catalysis may take a place at the chiral pockets on the surface partially covered with tartaric acid. Also, in this model, there is likely a cooperative interaction between the adsorbed tartrate and β-ketoester species[8]. Regardless, the lack of complexity of the individual chiral modifier in this case must be compensated by the intervention of several molecules.

In our research group, the adsorption of (S)-(-)-1-(1-naphthyl)-ethylamine ((S)-NEA) on Pt(111) surface was studied[9]. (S)-NEA is a chiral molecule capable to induce a modest degree of enantioselectivity to the hydrogenation of α-ketoesters using platinum catalysts[10]. (S)-NEA has some of the features responsible for chiral modification in cinchona alkaloids, including a chiral center bonded directly to an aromatic ring that facilitates adsorption. It was determined that adsorption of (S)-NEA on single crystal Pt(111) surface under UHV leads to an enhancement in the extent of the uptake of (S)-propylene oxide ((S)-PO), a chiral probe, compared to R-propylene oxide ((R)-PO). Figure 2.1 shows the chemical structures of (S)-NRA, (R)-(+)-1-(1-naphtyl)-ethylamine ((R)-NEA), (S)-PO and (R)-PO.

RAIRS uptake of S-NEA on Pt(111) suggested molecular adsorption. At low coverage (< 1.0 L), adsorption with the naphthalene ring standing up along its short axis on the surface is suggested. At high coverage (> 1.0L) adsorption geometry with the ring tilted away from the surface normal and standing up along its long axis on the surface is suggested. These nonflat adsorption states of the NEA may have important implications for its ability to impart surface chirality[9].

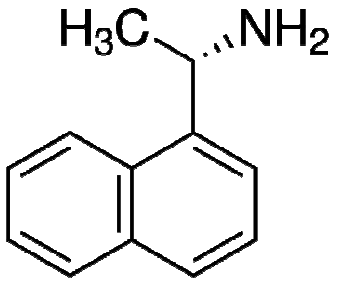

(S)-(-)-1-(1-Naphthyl)ethylemine

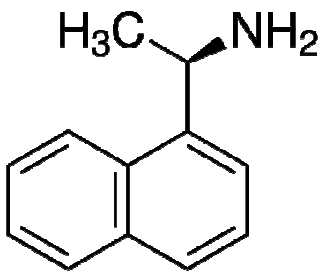

(R)-(+)-1-(1-Naphthyl)ethylemine

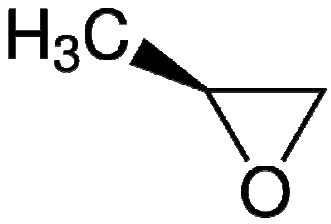

(S)-(-)-Propylene oxide

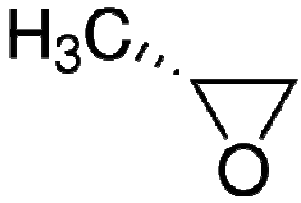

(R)-(+)-Propylene oxide

Figure. 2.1. Chemical structures

It was concluded that PO and (S)-NEA coadsorption experiments provide evidence for both supramolecular templating and individual complexation as possible mechanisms for the enantioselective adsorption enhancement.

On the other hand, Bonello et.al. employed scanning tunneling microscope (STM) and visually observed (S)-NEA covered Pt(111) surface and they did not observe ordered structure, which denies supramolecular templating model[11].

In order to further investigate this issue, in this study, RAIRS and TPD experiments were conducted with (R)-NEA instead of (S)-NEA.

2.2. Experimental

TPD and RAIRS experiments reported here were done in a two-level UHV chamber. The system was cryopumped to a base pressure around 2×10^{-10} Torr. The TPD experiments were conducted in the main chamber using a UTI 100C quadruple mass spectrometer retrofitted with a retractable nose cone ending in a 5 mm diameter aperture for the selective detection of the desorbing molecules from Pt surface. A constant heating rate of 10 K/s and a bias voltage of -100 V was applied to the crystal in order to repel any stray electrons. The RAIRS experiments were carried out in the second level of the chamber. The IR beam from a Bruker Equinox 55 FT-IR spectrometer was directed through polarizer and into the UHV chamber through NaCl window, focused onto the sample at grazing angle (~85°), sent back to the atmospheric side through another NaCl window, and focused onto a mercury-cadmium-telluride (MCT) detector. Spectra were obtained by averaging 2000 scans taken with 4 cm^{-1} resolution. Background spectra were obtained in a similar way for the clean surface prior to any gas dosing. The Pt(111) single crystal was mounted on the manipulator that can be cooled to ~80 K and resistively heated to 1100 K. A chromel-alumel thermocouple spot welded to the side of crystal was used for temperature measurement. The surface was routinely cleaned by cycles of Ar^+ sputtering, oxidation in 2×10^{-6} Torr of oxygen at 700 K, and annealing in vacuum at 1100 K. Gas exposures were performed by backfilling of the chamber. Gas dosing was done at liquid nitrogen temperature unless otherwise indicated.

The (R)-(+)-NEA (99.99 % purity) and (R)- and (S)-PO (both 99 % purity) were all purchased from Aldrich, purified via repeated freeze-pump-thaw vacuum distillation cycles before use, and

checked by mass spectroscopy. H_2 gas (99.999 % purity) was supplied by Liquid Carbonic and used as received.

2.3. Results

Fig. 2.2 shows RAIRS of (R)-NEA adsorbed on single-crystal Pt(111) surface at 80 K under UHV as a function of exposure. Table 2.1 shows the RAIRS peak assignments. The positions of peaks observed are close to those for the pure liquid, suggesting molecular adsorption. Essentially the same results were observed as RAIRS of (S)-NEA, therefore it is suggested that the adsorption state is the same for (S)- and (R)-NEA.

Fig 2.3 and 2.4 show TPD traces from coadsorption of various amounts of (R)-NEA and 2.0 L of (R)-PO and (S)-PO, respectively. Here the peaks observed are quite different from what was observed for (S)-NEA[9]. Two peaks can be easily identified at around 140 and 180 K. As the exposure of (R)-NEA increases, smaller peak at 180 K and larger peak at 140 K were observed. Based on this observation, it seems to be that the peak at around 140 K is multilayer desorption peak and the peak at around 180 K is monolayer desorption peak.

Compared to the experiments with (S)-NEA, no sharp dip between multilayer peak and only one peak for monolayer peak was observed instead of two, suggesting no strong interaction between NEA and PO. Also, compared to the experiments with (S)-NEA, there is a clear shift from monolayer desorption to multilayer with increasing (R)-NEA. Almost no multilayer desorption peak was observed with small (R)-NEA exposure, and almost no monolayer peak was observed with large (R)-NEA exposures.

In order to determine the peak area of monolayer and multilayer peak, the peaks were deconvoluted. From Fig. 2.3 and 2.4 both peaks seem to be somewhat tailing. Therefore the peaks were deconvoluted into four peaks accounting for tailing. Fig. 2.5 shows the result of peak

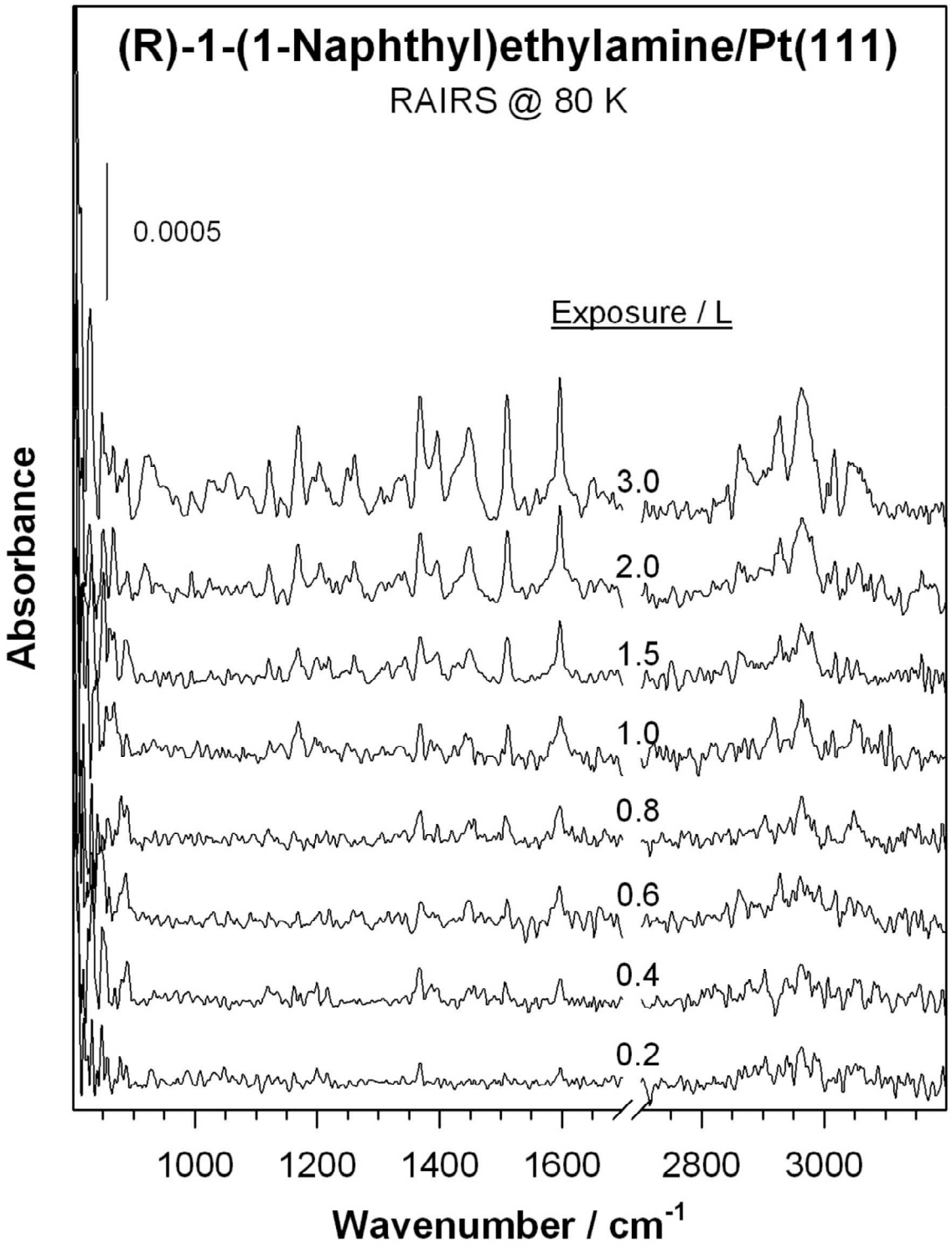

Figure 2.1. RAIRS for (*R*)-NEA adsorbed on a single-crystal Pt(111) surface at 80 K under UHV as a function of initial exposure.

Table 2.1. Vibrational Assignments of the Peaks in the RAIRS Data for Pure NEA and for NEA Adsorbed on Platinum Surfaces[a]

	NEA/Pt(111), UHV		NEA/Pt, from CCl_4		
mode	exposure <1.0 L	exposure >1.0 L	(*S*) or (*R*)	racemic	pure liquid
$\delta_{oop}(CH)_{ring\text{-}n}$	865 (w)	865 (s)			861 (s)
$\rho(CH_3)$	920 (m)	922 (m)			917 (m)
$\delta_{oop}(CH)_{ring\text{-}n}$		930 (m)	1102 (vs)	1105 (s)	
$\delta_{ip}(CH)_{ring\text{-}n}$		1121 (s)	1120 (m)	1128, 1132 (w)	1119 (s)
$\delta_{oop}(CH)_{ring\text{-}s}$	1168 (w)	1169 (s)	1162 (m)	1172 (m, br)	1167 (s)
$\delta_{ip}(CH)_{ring\text{-}s}$	1200 (m)	1205 (w)	1198 (m)	1218 (m)	1201 (w)
$\delta_{ip}(CH)_{ring\text{-}s}$		1242 (w)			1242 (w)
$\delta_{ip}(CH)_{ring\text{-}n}$	1257 (m)	1260 (m)	1253 (m)	1253, 1266 (s)	1259 (m)
$\delta(CH)_{EtNH_2}$		1325 (w)	1329 (m)	1323 (m)	1325 (sh)
$\delta(CH)_{EtNH_2}$		1343 (m)	1344 (w)	1345 (m)	1337 (m)
$\delta_s(CH_3)_{EtNH_2}$	1369 (s)	1369 (vs)	1374 (m)		1368 (vs)
$\nu_{ip}(CC)_{ring}$		1396 (m)	1398, 1408 (w)	1403 (m)	1395 (m)
$\delta_a(CH_3)_{EtNH_2}$	1432, 1448 (m)	1446 (s, br)	1443 (w)		1446 (s,br)
$\nu_{ip}(CC)_{ring\text{-}s}$	1510 (w)	1511 (vs)	1520 (vs)	1518, 1578 (s)	1510 (vs)
$\nu_{ip}(CC)_{ring\text{-}y}$	1600 (m)	1597 (vs)	1601 (s)	1598 (s)	1595 (vs)
$\nu_{ip}(CC)_{ring}$	1622 (w)	1620 (sh)	1620 (s)	1618 (s)	
$\nu_s(CH_3)_{EtNH_2}$	2866 (w)	2866 (m)		2870 (m, br)	2867 (m)
$\nu_a(CH_3)_{EtNH_2}$		2922 (m)	2917 (s, br)	2900 (m, br)	2922 (m)
$\nu_{ip,s}(CH)_{ring}$	2970 (vw)	2960 (vs)	2972 (s)	2962, 2972 (w)	2961 (vs)
$\nu_{ip,a}(CH)_{ring}$		3043 (w)	3011, 3032 (m)	3035 (w, br)	3047 (w)
$\nu_{ip,a}(CH)_{ring}$		3059 (m, br)	3065, 3077 (w)	3075 (w, br)	3063 (sh)

[a] All values are reported in cm^{-1}. Modes: ν = stretching, δ = deformation, ρ = rocking. Subindices: ip = in-plane, oop = out-of-plane, s = symmetric, a = asymmetric, $EtNH_2$ = ethylamine moiety, ring = naphthalene ring, ring-n = nonsubstituted benzene side of naphthalene, ring-s = substituted benzene side of naphthalene, ring-*y* = dipole along short axis of naphthalene ring plane, ring-*x* = dipole along long axis of naphthalene ring plane. Intensities: vs = very strong, s = strong, m = medium, w = weak, vw = very weak, sh = shoulder, br = broad.

Reprinted from ref. 9. Copyright (2008) American Chemical Society.

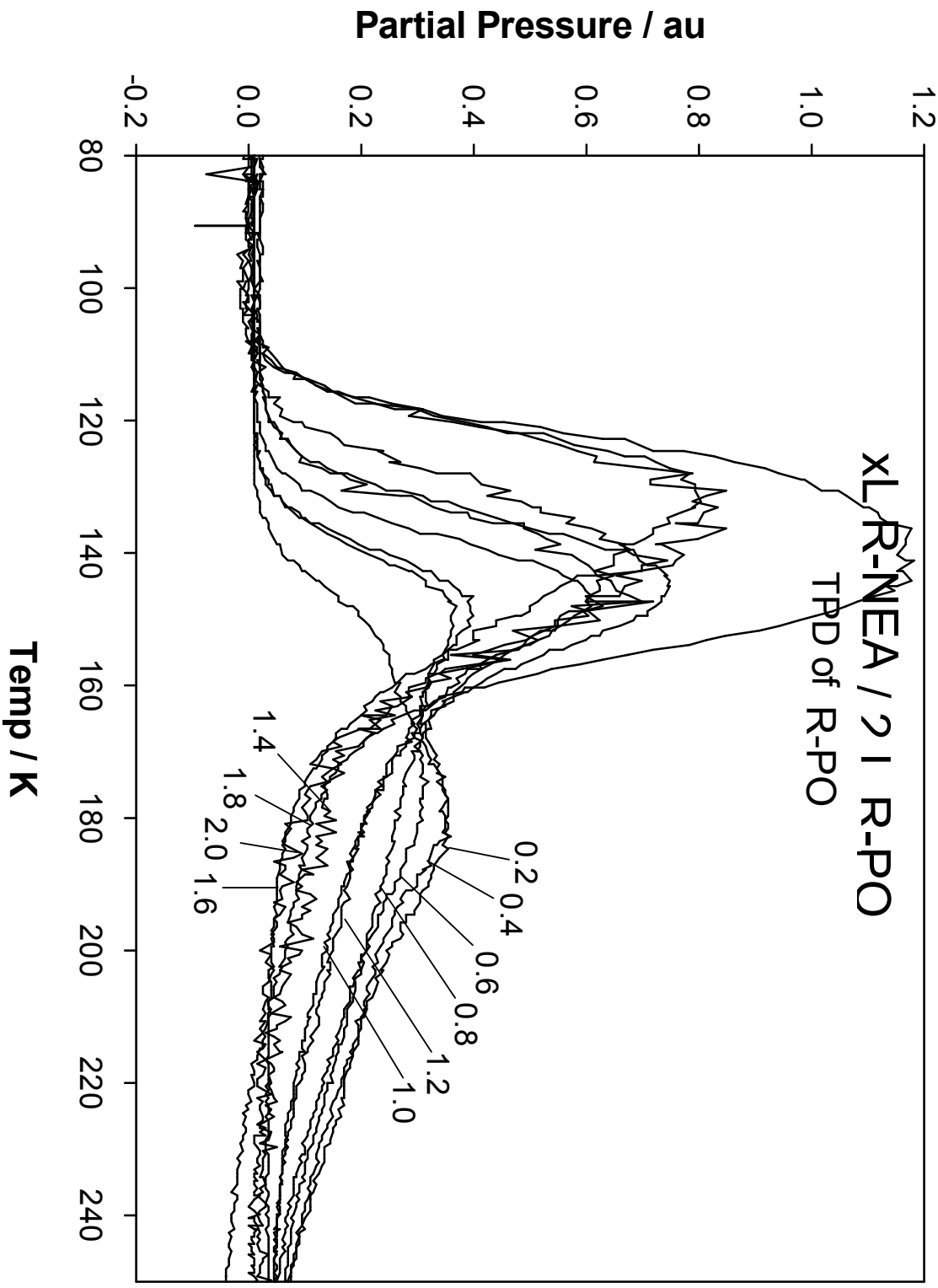

Figure 2.2. PO-titration TPD traces from Pt(111) surfaces first dosed with various amounts of (*R*)-NEA and then with 2.0 L of (*R*)- PO at liquid nitrogen temperatures.

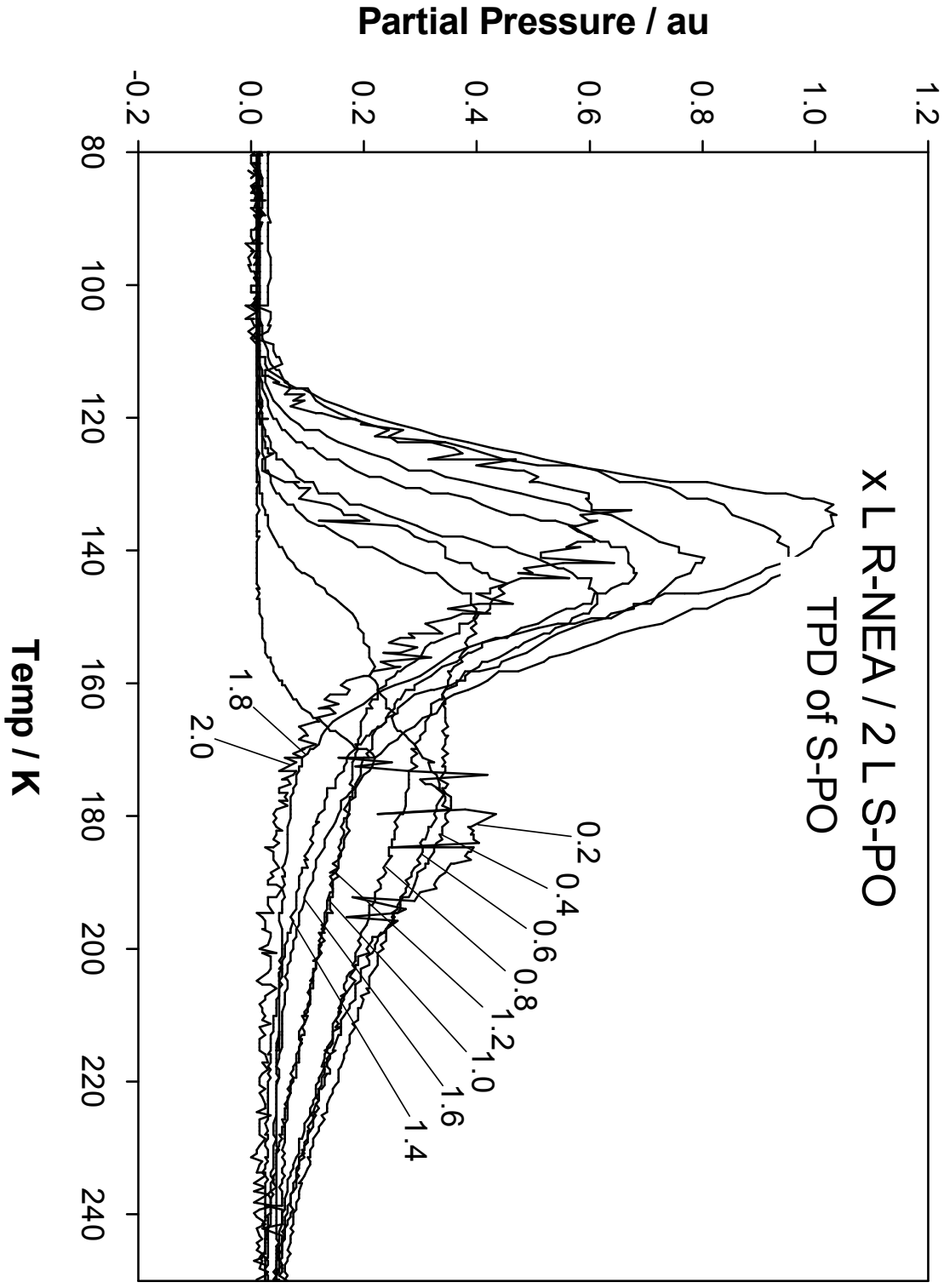

Figure 2.3. PO-titration TPD traces from Pt(111) surfaces first dosed with various amounts of (*R*)-NEA and then with 2.0 L of (*S*)- PO at liquid nitrogen temperatures.

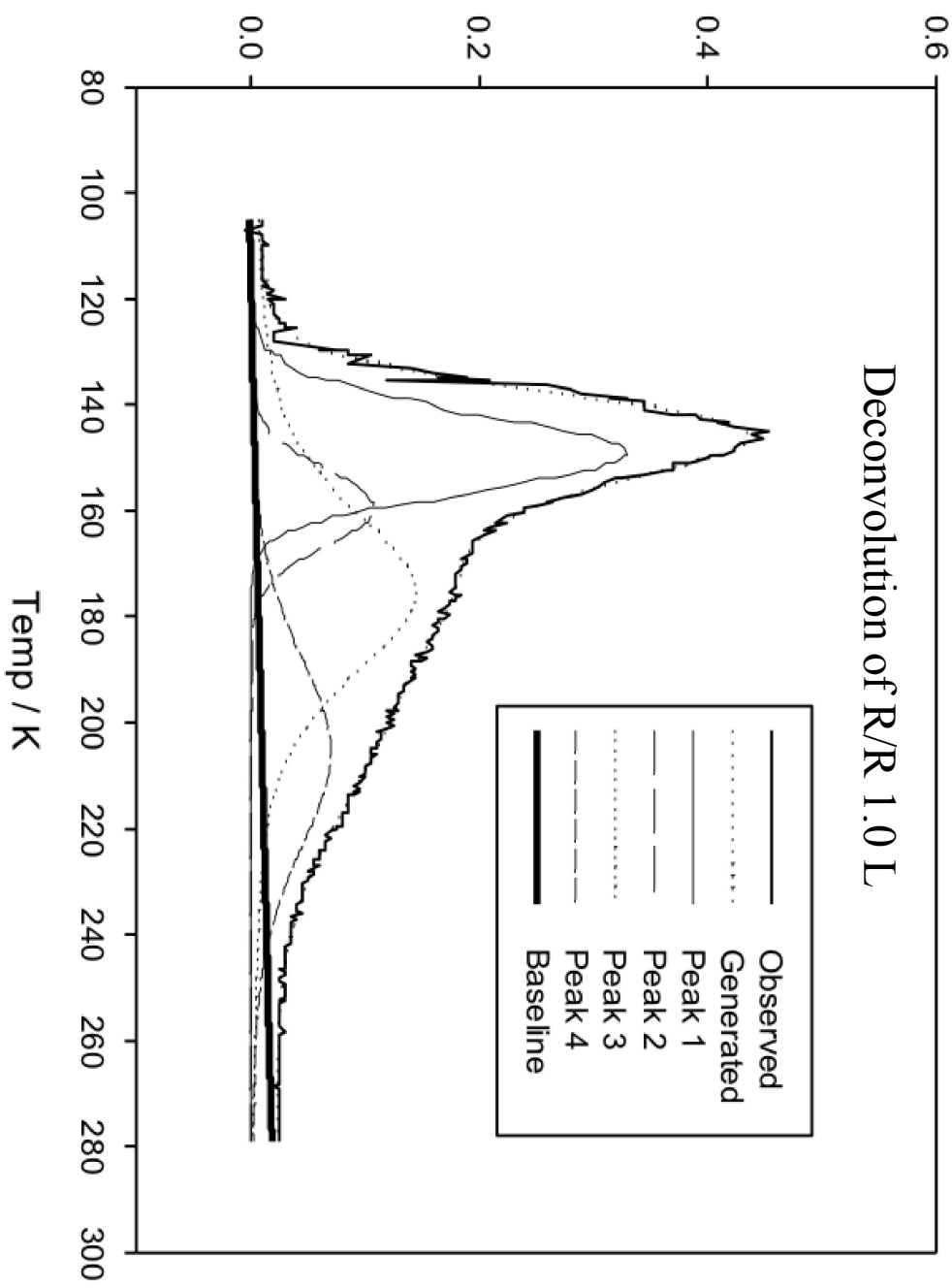

Figure 2.4. An example of deconvolution result (1.0 L of (R)-NEA and 2.0 L of R-PO)

Table 2.2. Decombolution Data of R/R pair

Peak No.	1		2		3		4	
Esposure	T	A	T	A	T	A	T	A
0.2	147	4.5	159	2.5	179	**12**	210	**9**
0.4	150	1.7	162	2.7	179	**11**	212	**7.2**
0.6	145	4	155	3	176	**11**	208	**5**
0.8	144	7.4	155	6.6	181	**9.4**	214	**4.6**
1	143	5.9	154	2.1	170	**7.9**	202	**4.1**
1.2	141	9.5	155	6.8	177	**6.8**	208	**3.6**
1.4	136	9.3	148	11	175	**4.7**	210	**2.4**
1.6	127	9.4	141	13	159	**2.5**	175	**1.2**
1.8	133	24	150	23	181	**1.9**	204	**0.8**
2	131	15	149	14	174	**0.8**	-	**0**

T: Peak top temperature, A: Peak area

Table 2.3. Decombolution Data of R/S pair

Peak No.	1		2		3		4	
Esposure	T	A	T	A	T	A	T	A
0.2	-	0	-	0	182	**11.9**	212	**7.3**
0.4	151	18	168	1.1	179	**11.5**	210	**6.5**
0.6	147	5.4	167	9.7	186	**8.8**	214	**6.3**
0.8	145	9.3	162	8.9	183	**8.1**	208	**4.6**
1	143	5	152	4	172	**6.2**	204	**3.4**
1.2	142	9	155	9.6	183	**5.2**	211	**3**
1.4	138	12	152	10	176	**4.1**	209	**0.8**
1.6	135	14	149	17	177	**2.4**	203	**1.7**
1.8	133	10	148	7.5	175	**1.3**	204	**0.5**
2	134	14	147	15	178	**0.2**	-	

T: Peak top temperature, A: Peak area

Table 2.4. Area of monolayer desorption peak

	RR			RS		
exposure	Peak 3	Peak 4	sum	Peak 3	Peak 4	sum
0.2	12	9	19	11.9	7.3	19.2
0.4	10.8	7.3	18.1	11.5	6.5	18
0.6	11	5	16	8.7	6.3	15
0.8	9.4	4.6	14	8.1	4.6	12.7
1	7.8	4.1	11.9	6.2	3.4	9.6
1.2	6.8	3.6	10.4	5.2	3	8.2
1.4	4.7	2.4	7.1	4.1	0.8	4.9
1.6	2.5	1.7	4.2	2.4	1.7	4.1
1.8	1.9	0.8	2.7	1.3	0.5	1.8
2	0.8	0	0.8	0.2	0	0.2

deconvolution. The sum of peaks 1 and 2 is considered to be the multilayer peak and the sum of peaks 3 and 4 is considered to be the monolayer peak. Table 2.2 and 2.3 show the peak temperature and peak area for RR and RS pair. No clear difference was observed in the peak temperature between RR and RS pair, which is different from the experiments with (S)-NEA[9].

Fig. 2.5 shows the relationship between (R)-NEA exposure and monolayer peak area. In general, PO yields decreased as the NEA coverage increased. However a slight deviation from this trend was seen at intermediate (R)-NEA exposures with (R)-PO (RR pair). This is basically the same as the results seen for SS pair, although this deviation is much less. Considering the fact that controlling NEA exposure was quite difficult, this deviation may not be meaningfully large.

The effect of coadsorbed (R)-NEA on the uptake of (S)- and (R)-PO was also studied with RAIRS. As shown in Fig. 2.6, almost no difference was observed between RS pair and RR pair.

Fig. 2.7 is the details of one frequency region of Figure 2.6, corresponding to the main PO ring deformation mode. The peak can be deconvoluted into monolayer peak and multilayer peak. Table 2.5 shows the results from this deconvolution. When (R)-NEA exposure is 0.4 L, the peak area of monolayer peak in RR and RS are almost the same. On the other hand, when (R)-NEA exposure is 1.0 L, the peak area of monolayer peak in RR is larger than that in RS. These results are basically the same as that in the experiment with (S)-NEA, which supports the idea of supramolecular templating by NEA molecules. However peak shape in RAIRS is not so reproducible in general, and also this set of experiments was conducted only once. Therefore this may not be a solid piece of evidence for the templating model by NEA.

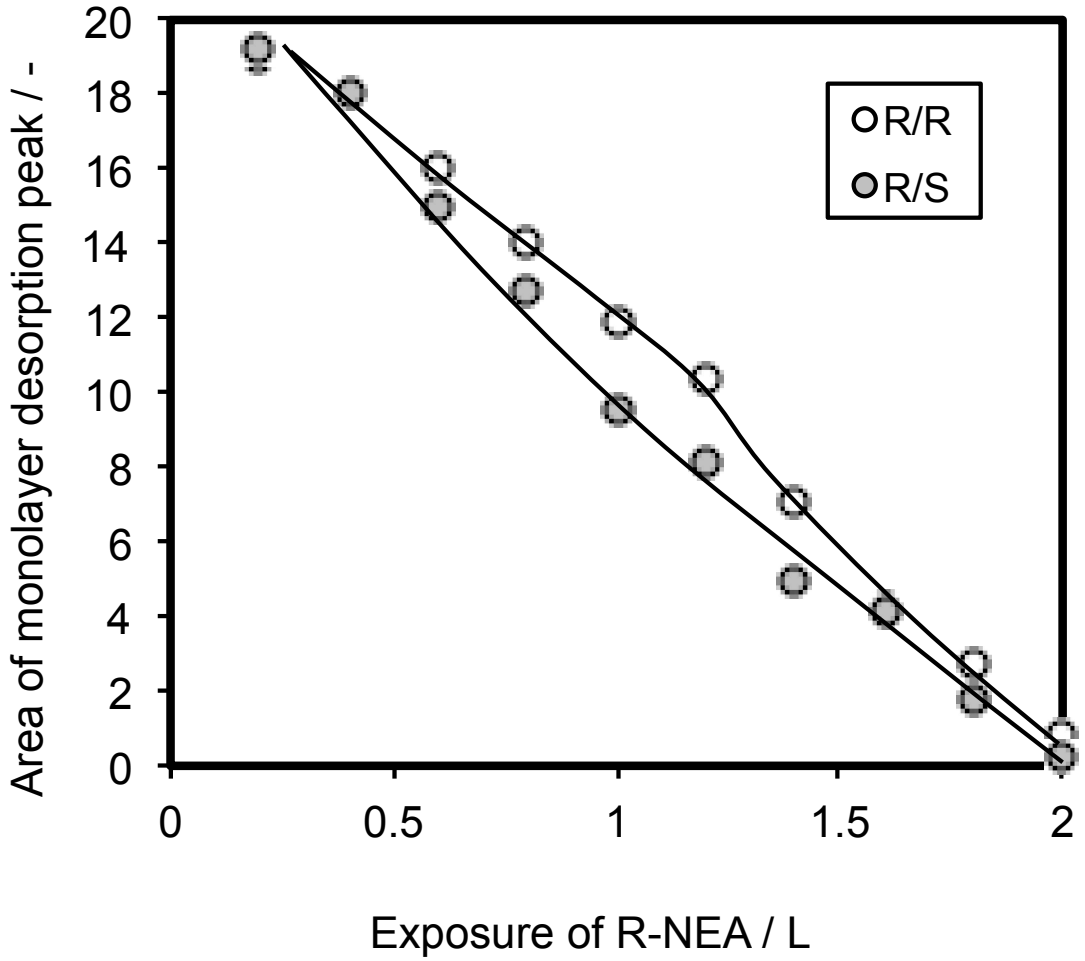

Figure 2.5. Monolayer PO desorption yields, estimated from the TPD titration experiments in Figure 2.3 and 2.4, as a function of initial (*R*)-NEA exposure.

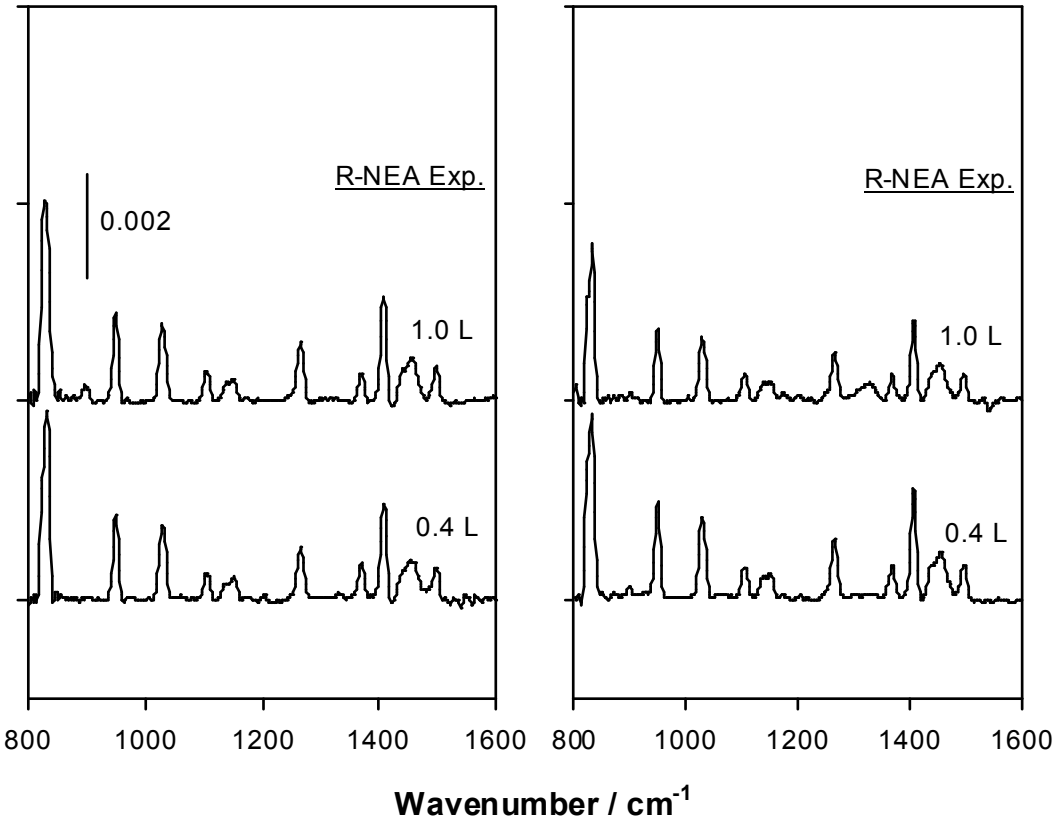

Figure 2.6. RAIRS from Pt(111) surfaces first exposed to various amounts of (*R*)-NEA and then to 1.0 L of (*S*)- or (*R*)-PO.

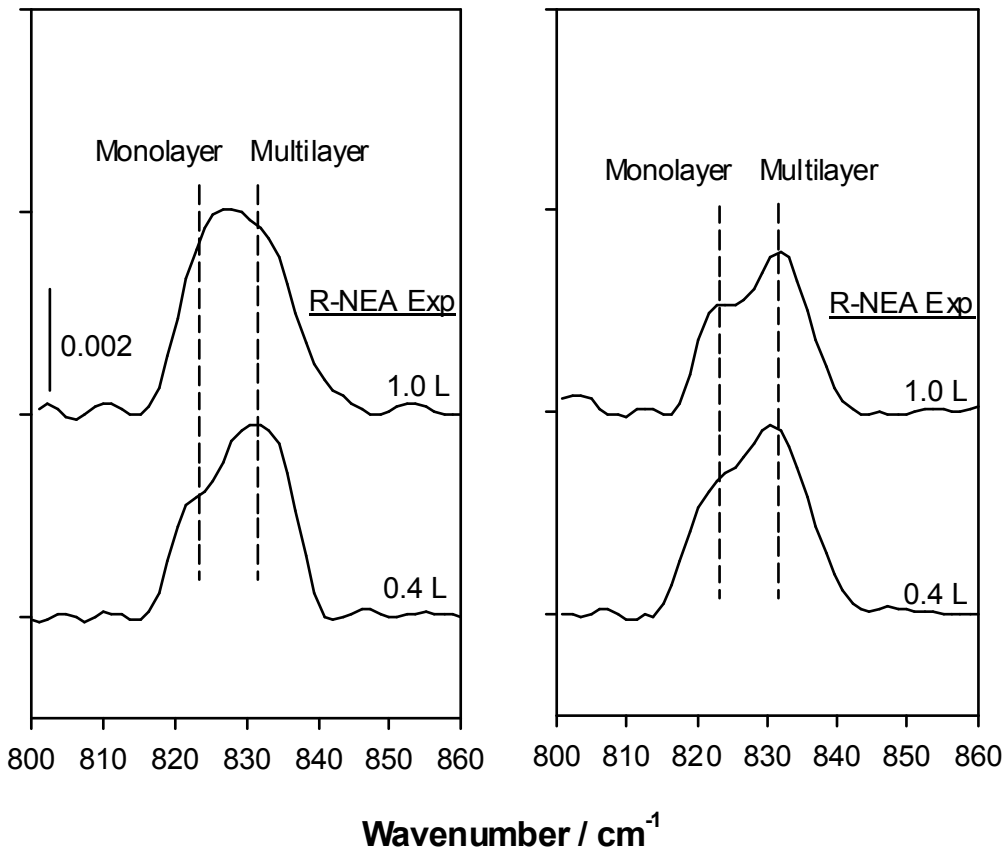

Figure 2.7. Details of the RAIRS data in Figure 2.11, highlighting the signals from the ring-deformation mode of PO. Two peaks are seen for that mode at 825 and 832 cm-1, corresponding to monolayer and multilayer adsorption, respectively.

Table 2.5. Deconvolution of ring deformation peak

		Monolayer		Multilayer	
	NEA exposure	Wavenumber	Peak area	Wavenumber	Peak area
RR	0.4	822	0.802	831	2.158
	1.0	824	1.058	831	2.306
RS	0.4	821	0.803	831	2.329
	1.0	822	0.632	832	1.798

2.4. Conclusions

The main observations in the experiments mentioned above are:

1. RAIRS for (R)-NEA seems almost the same as that for (S)-NEA.
2. Only one monolayer desorption peak of PO was observed in TPD of both (R)-NEA and PO. Also, there was no difference in desorption peak temperatures in TPD between RR and RS pair. These two facts strongly suggest that there is no 1:1 interaction between (R)-NEA and (R)-PO.
3. No sharp drop between multilayer and monolayer peak was observed.
4. A clear gradual shift from monolayer peak to multilayer peak was observed as (R)-NEA exposure was increased.
5. Slight enantioselective enhancement of (R)-PO adsorption compared to (S)-PO when the surface is partially covered (~1 L) was observed in both RAIRS and TPD, suggesting templating model of (R)-NEA.
6. Almost no other difference was seen in RAIRS of RR pair and RS pair.

From the viewpoint of the effect of (S)-NEA and (R)-NEA, mixed results were obtained. Enantioselective adsorption enhancement was observed for both SS pair and RR pair in both TPD and RAIRS, suggesting templating model as a possible explanation for chiral catalysis. No evidence for 1:1 complex formation was observed in the experiment with (R)-NEA. It would be very strange if a 1:1 complex formation only occurs with SS pair but not with RR pair.

Overall, controlling NEA exposure was very difficult and the error bars in the experiments mentioned above seem to be fairly large. Therefore, observed enantioselective adsorption enhancement in RR pair may not be meaningfully large.

2.5. References

(1) Blaser, H. U.; Spindler, F.; Studer, M. *Applied Catalysis A: General* **2001**, *221*, 119–143.
(2) Murzin, D. Y.; Mäki Arvela, P.; Toukoniitty, E.; Salmi, T. *Catalysis Reviews* **2005**, *47*, 175–256.
(3) Izumi, Y. *Advances in Catalysis*; Advances in Catalysis; Elsevier, 1983; Vol. 32, pp. 215–271.
(4) Webb, G.; Wells, P. B. *Catalysis today* **1992**, *12*, 319–337.
(5) Studer, M.; Blaser, H.-U.; Exner, C. *Advanced Synthesis & Catalysis* **2003**, *345*, 45–65.
(6) Bonalumi, N.; Bürgi, T.; Baiker, A. *J. Am. Chem. Soc.* **2003**, *125*, 13342–13343.
(7) Osawa, T.; Harada, T.; Takayasu, O. *Current Organic Chemistry* **2006**, *10*, 1513–1531.
(8) Jones, T.; Baddeley, C. *Surface Science* **2002**, *519*, 237–249.
(9) Lee, I.; Ma, Z.; Kaneko, S. *Journal of the American Chemical Society* **2008**, *130*, 14597–14604.
(10) Minder, B.; Schürch, M.; Mallat, T.; Baiker, A.; Heinz, T.; Pfaltz, A. *Journal of Catalysis* **1996**, *160*, 261–268.
(11) Bonello, J. M.; Williams, F. J.; Lambert, R. M. *J. Am. Chem. Soc.* **2003**, *125*, 2723–2729.

Chapter 3: Hydrogenation reactions on Shape Controlled Particles

3.1. Introduction

It has been long recognized that there is the effect of structural factors in heterogeneous catalysis[1,2]. Most of solid catalysts consist of finely dispersed active phase, typically an expensive transition metal, and porous high-surface-area metal oxide support. The supported metal particles show a wide variety of shapes, and therefore many surface structures. UHV studies with single crystal surfaces have shown that different surface planes can show widely different chemistries. For instance, activation rate of nitrogen varies drastically on different planes of iron surfaces[3,4]. These differences suggest that controlling surface structure can potentially control the catalytic selectivity. However, this promise has yet to be fully realized due to the difficultly in preparing supported catalysts with well-defined surface structure.

It has been reported from our research group that tuning reaction selectivity in a real catalytic system was indeed possible through the specific control of particle shape. Our example is the selective isomerization of trans olefins to their less thermodynamically favored cis conformation[5,6,7,8].

In this project, the aim was to test if the effect of particle shape can be seen in the product distribution in hydrogenation reaction that results in two or more possible hydrogenation products. Hydrogenation has been also known as structure insensitive reaction, however, if the particle shape affects the isomerization reaction rate between cis and trans isomers, it can also affect the product distribution in hydrogenation reaction.

In order to test this hypothesis, hydrogenation of isoprene was studied with shape-controlled Pt catalysts. Isoprene has two double bonds and can be hydrogenated into three partial hydrogenation products, 3-methyl-1-butene (3M1B), 2-methyl-1-butene (2M1B), 2-methyl-2-butene (2M1B), and one total hydrogenation product, 2-methylbutane (2MB), as shown in Fig. 3.1.

This reaction has not been studied extensively in the past and only about ten publications could be found on hydrogenation of isoprene probably because it is not commercially attractive. Vassilakis et. al. reported the product distribution when Pt(111) was used as catalyst as shown in Fig. 3.2[9]. They mentioned that this product distribution is probably governed by the relative stability of adsorbed species. No one has reported that the analysis of surface species during hydrogenation of isoprene, but three adsorbed species shown in Fig. 3.3 should be the reasonable ones that lead to three partial hydrogenation products upon desorption. Expected adsorbed species to 3M1B has two carbons right above the surface and it seems to be sterically most hindered thus unstable, which can be a reasonable explanation for small selectivity into 3M1B compared to other two partial hydrogenation products. The idea was that the adsorption energy of these three species should be strongly affected depending on the exposed surface, therefore the shape of the catalyst particle, if it affects the adsorption energies of cis- and trans-butenes.

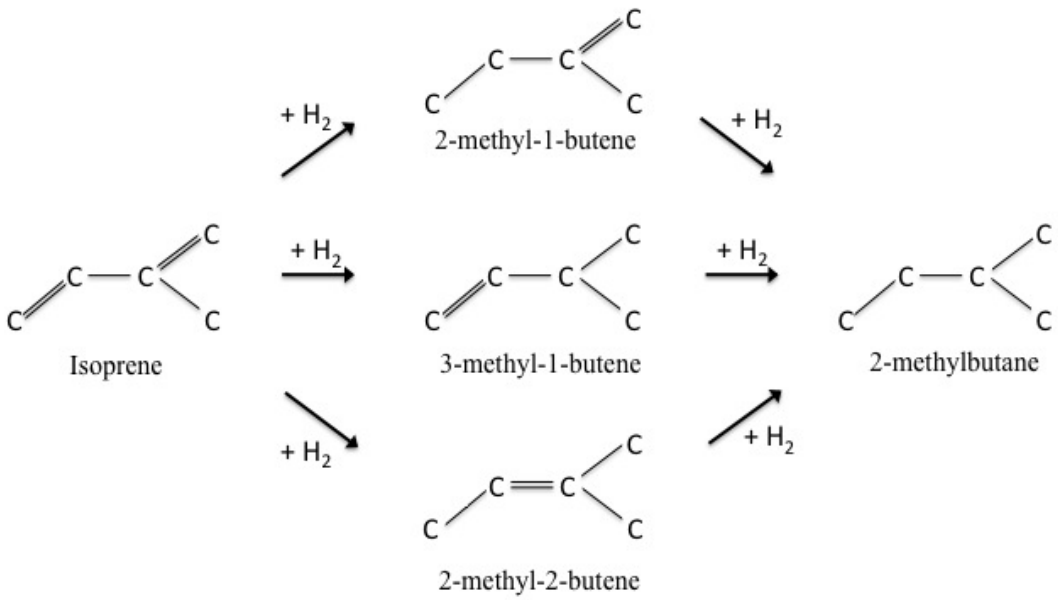

Figure 3.1. Hydrogenation of isoprene

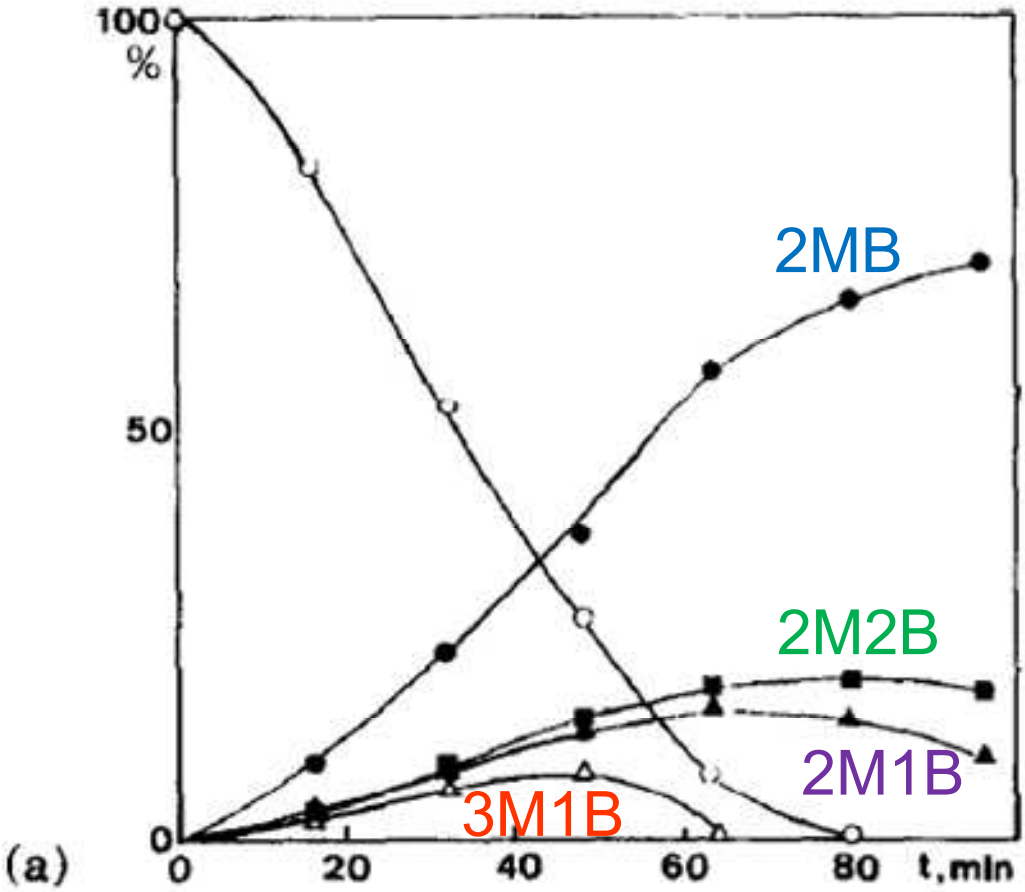

Figure 3.2 Reported reaction result of isoprene hydrogenation on Pt(111).

Reprinted from ref. 20. Copyright (1990) Elsevier.

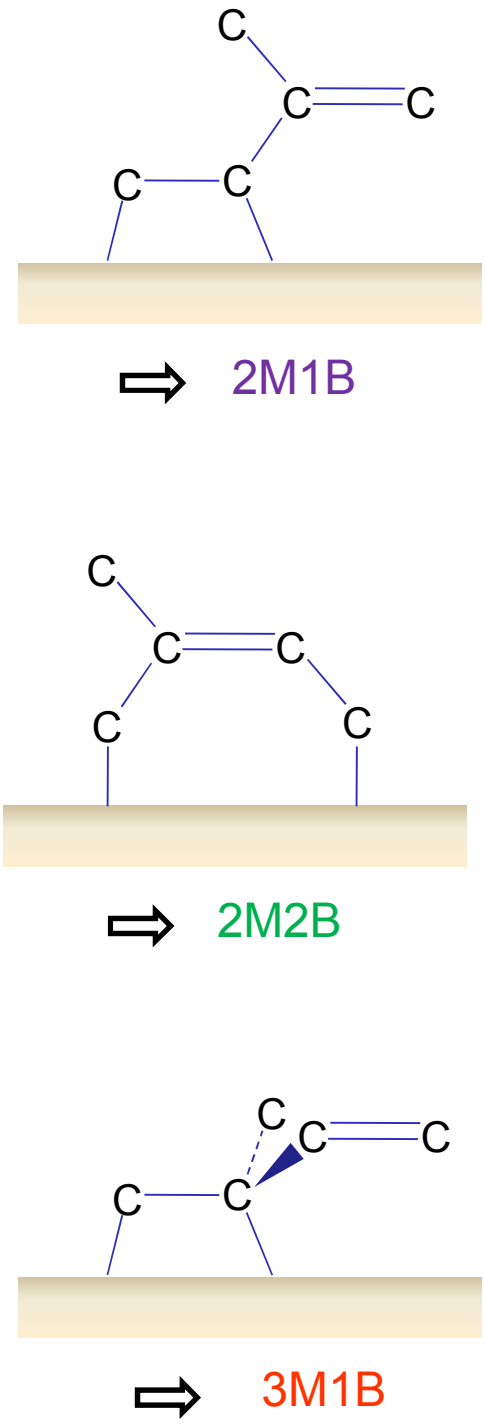

Figure 3.3 Expected adsorbed surface species into partial hydrogenation products

In order to test this hypothesis, hydrogenation of isoprene was conducted in a home-made gas-phase circulation reactor using shape-controlled colloidal supported Pt catalysts. Additionally, another gas-phase circulation reactor that was used for cis- and trans-2-butene isomerization was used for comparison.

Other hydrogenation reactions in which two or more possible hydrogenation products can be obtained were also tested in gas-phase circulation reactor. Particularly, hydrogenation of crotonaldehyde was investigated extensively[10,11,12]. Crotonaldehyde has both C=C and C=O double bond and has been an important model reactant to study what controls the hydrogenation of either C=C or C=O double bond as shown in Fig. 3.4. Also, crotylalcohol is a valuable intermediate for production of perfumes and pharmaceuticals. Grass et.al. employed Pt catalysts with various particle size (1.7 to 7.1 nm) and larger particle size resulted in higher selectivity to crotylalcohol (increased from 13.7 to 33.9 %)[10]. This effect of particle shape is believed to be strongly related to the exposed facet, therefore it is highly likely to observe some effect of particle shape on the product distribution.

The preparation of tetrahedral and cubic particles was conducted using the method that was developed for cis-trans isomerization reaction by Dr. Ilkeun Lee. The particle shape was monitored with transmission electron microscope. Selected batches of colloidal nanoparticles were deposited on SiO_2 xerogel that was produced by Dr. Ilkeun Lee.

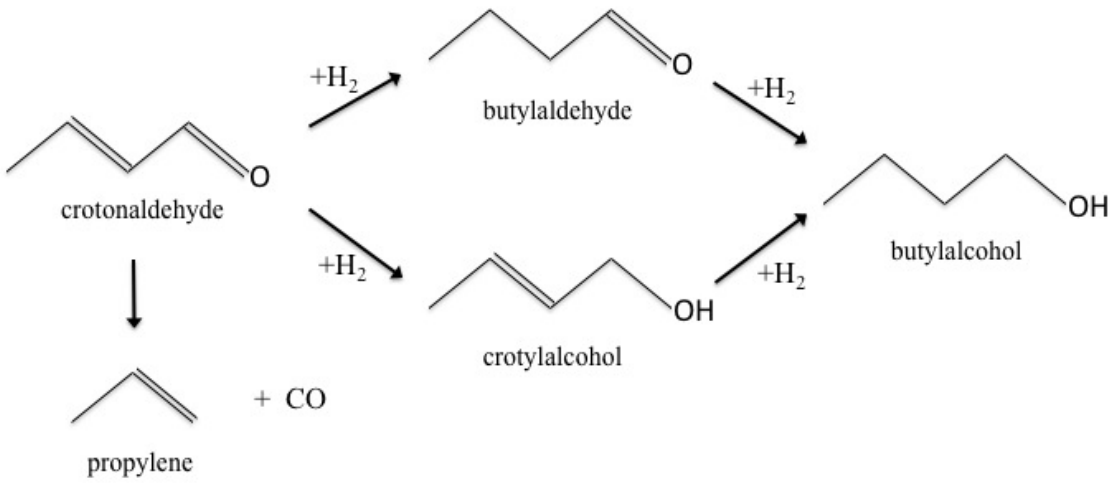

Figure 3.4. Hydrogenation of crotonaldehyde

3.2. Experimental

3.2.1. Preparation of catalysts

The catalysts employed in this study are Pt/SiO_2 prepared in a various methods. The catalyst prepared in a conventional impregnation method is named as normal catalyst, which is considered to be predominantly spherical shape. Tetrahedral catalysts were prepared in colloidal phase using $H_2PtCl_6 \cdot 6H_2O$ (99%, Alfa Aesar) and polyvinylpyrrolidone (PVP, Average M_W = 360,000). Cubic catalysts were prepared with K_2PtCl_4 (99.99 %) and sodium polyacrylate (SPA, Average M_W = 2,100). Prepared colloidal nanoparticles were deposited on SiO_2 xerogel prepared by Dr. Ilkeun Lee.

3.2.1.1. Preparation of normal Pt/SiO_2 catalysts

Desired amount of H_2PtCl_6 aq and SiO_2 (A200, Aerosil) were added in about 150 ml of distilled water. This solution was dried in a rotary evaporator. Obtained sample was dried in an oven at around 150 °C overnight. Dried sample was calcined in a muffle furnace at 300 °C for 3 hours. For comparison, catalysts calcined at 500 and 700 °C were also prepared.

3.2.1.2. Preparation of colloidal tetrahedral particles

Desired amounts of H_2PtCl_6 aq and PVP aq were added to milli-Q water, thoroughly mixed, treated with bubbling argon for 20 min, and reduced with bubbling hydrogen for 20 min. Then the container was filled with hydrogen, wrapped in aluminum foil, and stored in dark overnight.

3.2.1.3. Preparation of colloidal cubic particles

Desired amounts of K_2PtCl_4 aq and SPA aq were added to milli-Q water, thoroughly mixed, treated with bubbling argon for 20 min, and reduced with bubbling hydrogen for 20 min. Then the container was filled with hydrogen, wrapped in aluminum foil, and stored in dark overnight.

3.2.1.4. Deposition of colloidal particles on xerogel SiO_2

Xerogel prepared by Dr. Ilkeun Lee was employed. Desired amount of xerogel was added to colloidal solution, thoroughly mixed, left overnight, then filtered out. Obtained sample was dried in an oven at around 150 °C overnight. Pt loading was set to 0.5 wt%

3.2.2. TEM measurements

TEM measurements were performed on a Phillips TECNAI 12 TEM (120 kV accelerating voltage). The colloidal particles were deposited directly onto Cu grids covered with a carbon

support film (Ted Pella), and supported catalysts were dispersed in distilled water by ultrasonication and deposited from the resulting suspension onto the Cu grids.

3.2.3. Gas-phase circulation reaction

Fig. 3.5 shows the schematic of the reactor. The catalytic activity of supported Pt catalysts were investigated in a batch reactor consists of a stainless steel loop with ~180 ml total volume evacuated with a mechanical pump to a base pressure of 30 mTorr.

The catalyst was supported with two kinds of glass wools in a glass u-tube connected to the reactor. One is the glass wool that has been used in our research group. This glass wool has hard, coarse texture. This wool is referred as coarse wool in this thesis. Details about this wool are unknown because the label of the container is missing. This wool was employed in the reported cis-trans isomerization study cis- and trans-2-butenes. Additionally, silanized glass wool (Supelco) with soft and fine texture was employed in order to capture catalyst powder more securely. This wool is referred as silanized wool in this thesis.

Before the reaction, catalyst was dried in vacuum at 150 °C for 30 min and then reduced in hydrogen at 300 °C for 1 h unless otherwise noted.

After the pretreatment, the catalyst was cooled down to the desired temperature for the reaction. The reactor was evacuated to ~50 mTorr, then reactant gas (vapor), hydrogen and argon was introduced in the reactor. The gases were circulated with a circulation pump and fully mixed.

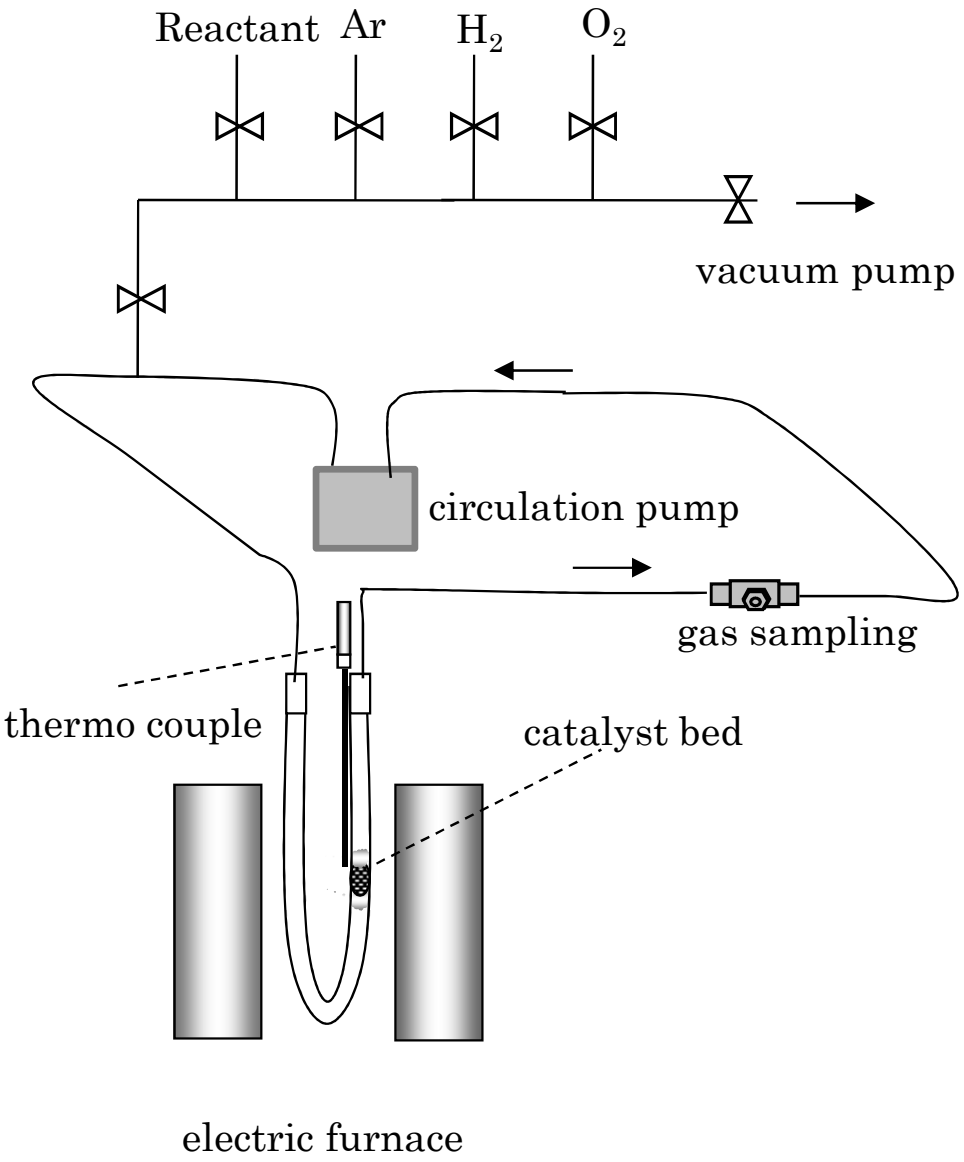

Figure.3.5 Gas-phase circulation reactor

Certain time after the beginning of the reaction, 0.1 ml of reaction gas was sampled from the septum using a gas tight syringe. Sampled gas was analyzed with a FID-GC 6890N (Agilent).

In some cases, the reaction was repeated after 1) evacuation of the reaction gas, 2) reduction, and 3) oxidation.

3.2.3.1 Hydrogenation of crotonaldehyde

Hydrogenation of crotonaldehyde was conducted with normal and silanized wool with reduction at 300 °C for 1h prior to the reaction. 10 Torr crotonaldehyde vapor, 100 Torr of hydrogen and 490 Torr of argon were employed for the reaction at 100 °C. DB-WAX was used at 80 °C for GC anlysis.

3.2.3.2. Hydrogenation of isoprene

Hydrogenation of isoprene was conducted with 1) both normal and silanized wool, 2) normal wool, 3) without wool. 10 Torr of isoprene, 100 Torr of hydrogen, and 490 Torr of argon were used at 50 °C. Chrompak PLOT Fused Silica column was used at 160 °C for GC separation. GC-MS with DB-5 column was also used for identification of the products.

3.2.3.3 Hydrogenation of other reactants

Hydrogenation was also conducted with various reactants. Acrolein, methyl vinyl ketone, acrylonitrile styrene, furan, pyrrole, acrylonitrile, pyruvonitrile, and 2-methylfuran were tested at

various temperatures (50-200 °C).10 Torr of reactant vapor, 100 Torr of hydrogen, and 490 Torr of argon were used. DB-WAX column was used for product analysis. GC-MS with DB-5 column was also used for product analysis in some cases.

3.3. Results

3.3.1. Hydrogenation of crotonaldehyde

3.3.1.1. Prepared catalysts

Hydrogenation of crotonaldehyde was conducted with normal Pt catalysts calcined at various temperatures (300, 500, and 700 °C), and supported tetrahedral catalyst prepared by Dr. Ilkeun Lee. Fig. 3.6-3.8 show TEM pictures of 0.5 wt% normal catalysts calcined at 300, 500, and 700 °C. The size of platinum particles increased after calcination at higher temperatures (~1, ~8, and ~15 nm). This set of catalysts can be used to test the effect of particle size on the reaction. Fig. 3.9 and Fig. 3.10 show TEM pictures of colloidal and supported tetrahedral catalysts prepared by Dr. Ilkeun Lee. Some particles seem to have defined tetrahedral shape before deposition, but this does not seem to be the case after deposition. There does not seem to be many tetrahedral particles. Some particles may have lost their defined shape during the deposition process. The average particle size is ~5nm and almost unchanged before and after deposition.

3.3.1.2. Hydrogenation

Hydrogenation of crotonaldehyde was conducted using the catalysts mentioned in the previous section in the gas-phase circulation reactor with both coarse and silanized wool. The catalysts were dried in vacuum at 150 °C for 30 min and reduced in 300 °C for 1h prior to the reaction.

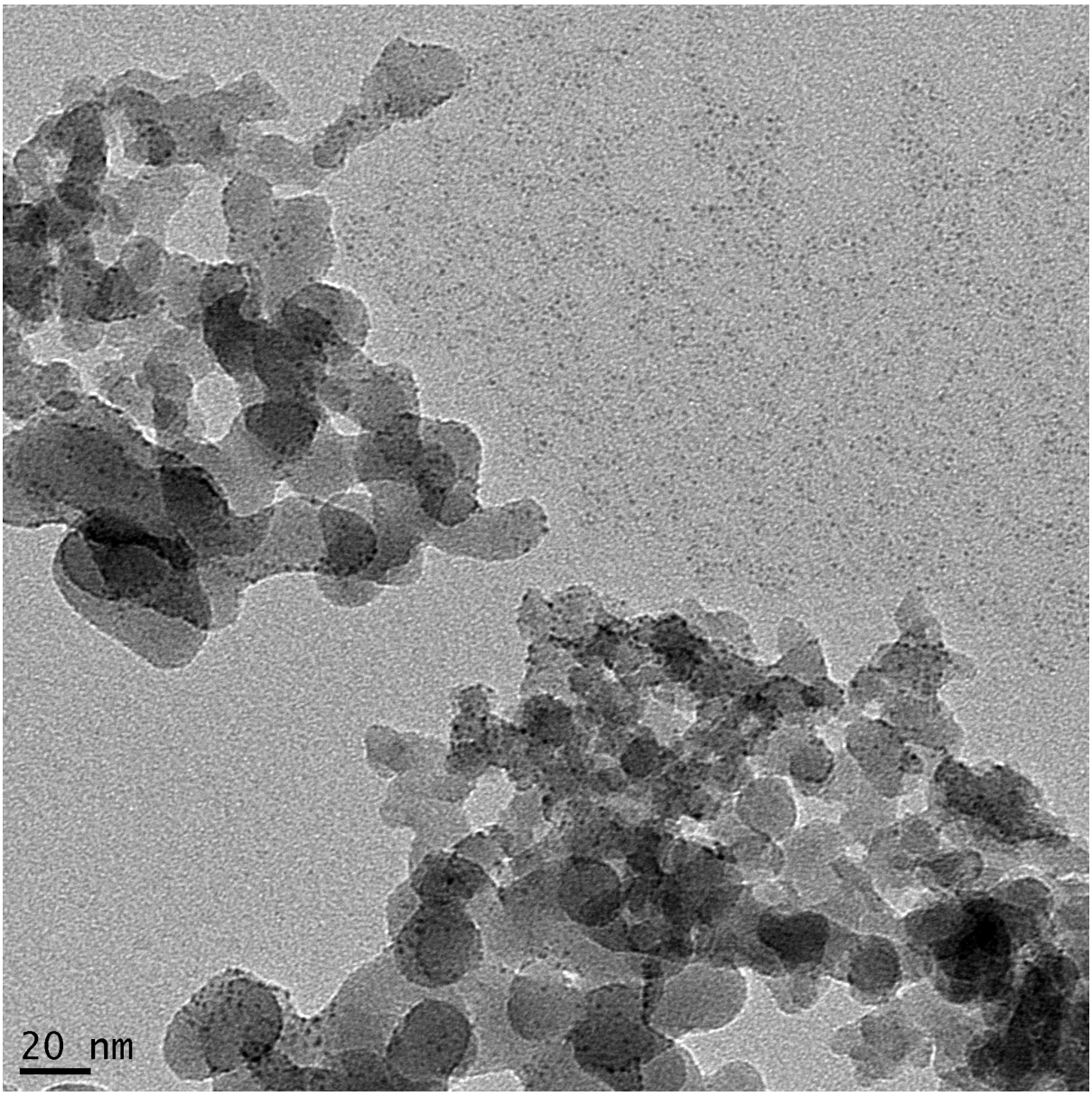

Figure 3.6 TEM image of 0.5 wt% normal Pt/SiO_2 calcined at 300 °C

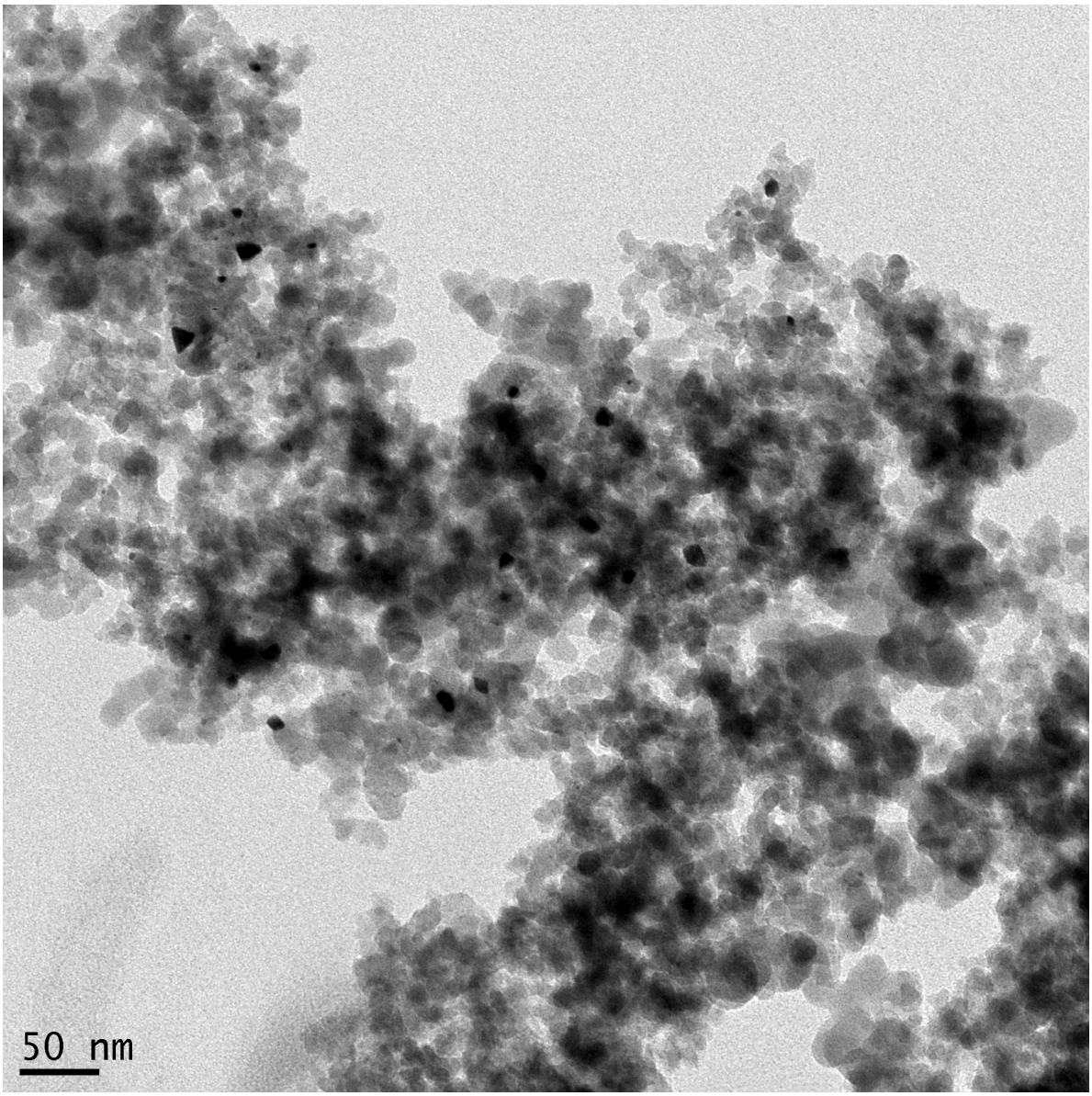

Figure 3.7 TEM image of 0.5 wt% normal Pt/SiO_2 calcined at 500 °C

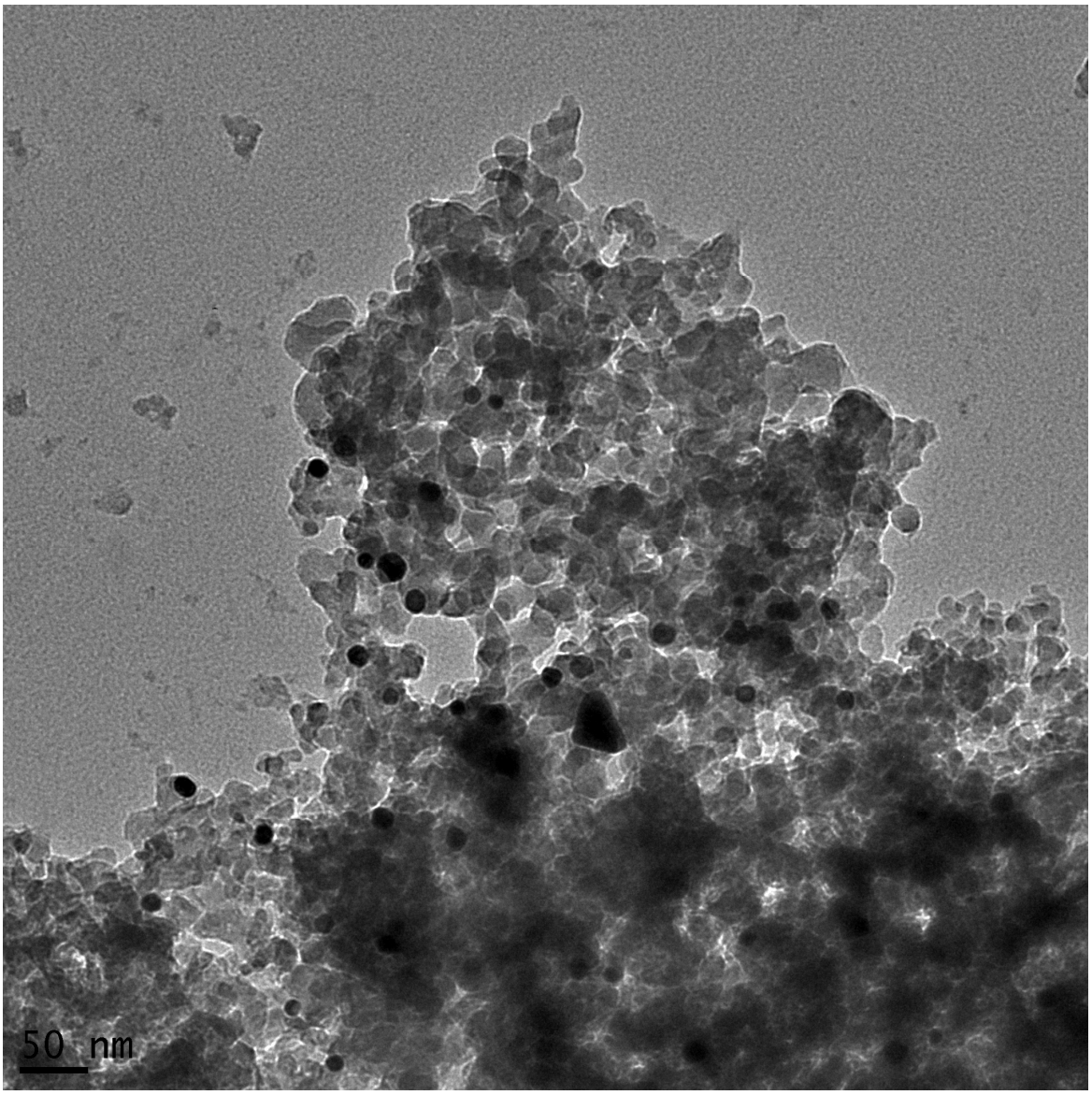

Figure 3.8 TEM image of 0.5 wt% normal Pt/SiO_2 calcined at 700 °C

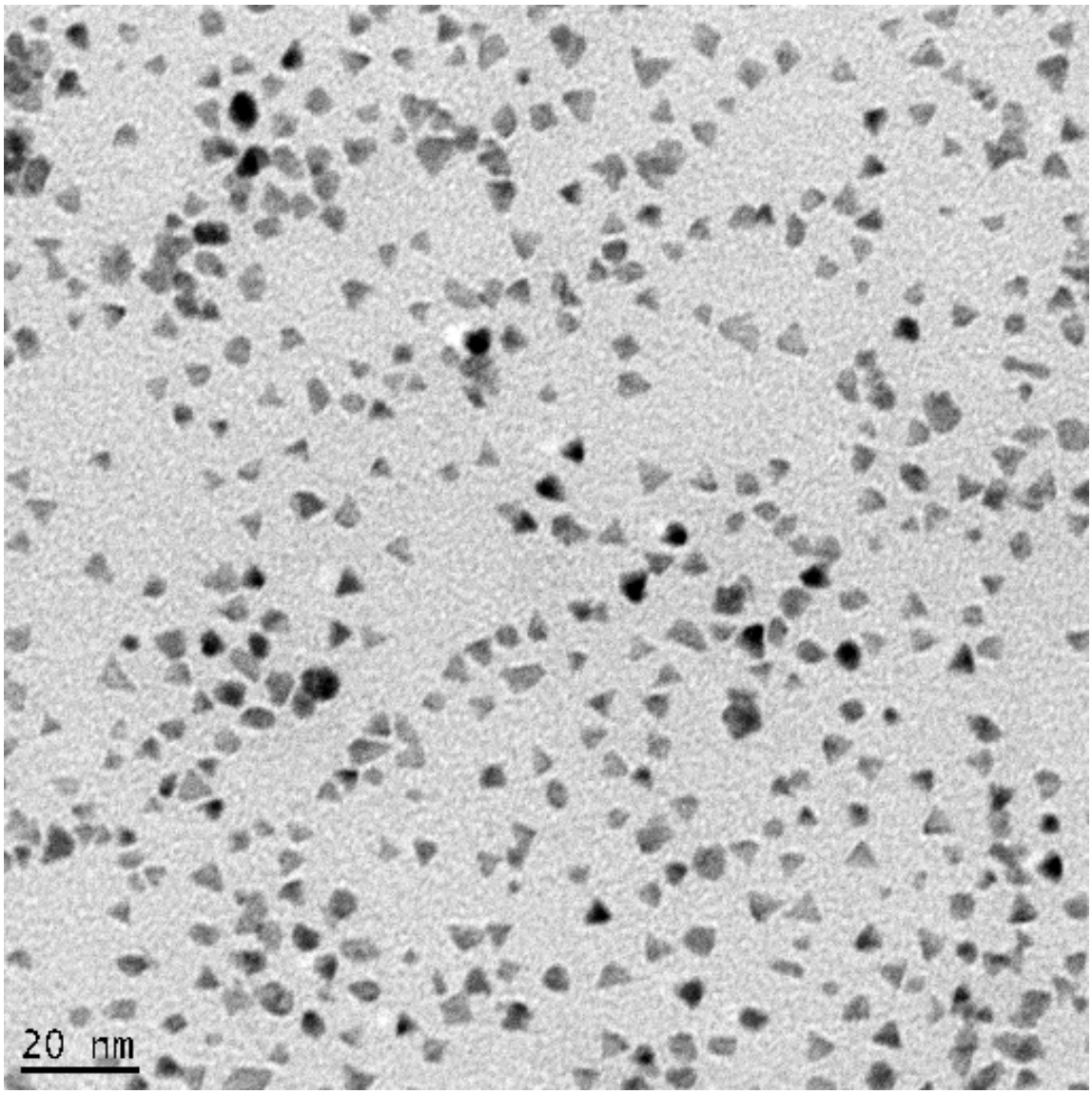

Figure 3.9 TEM image of colloidal tetrahedral particles prepared by Dr. Ilkeun Lee

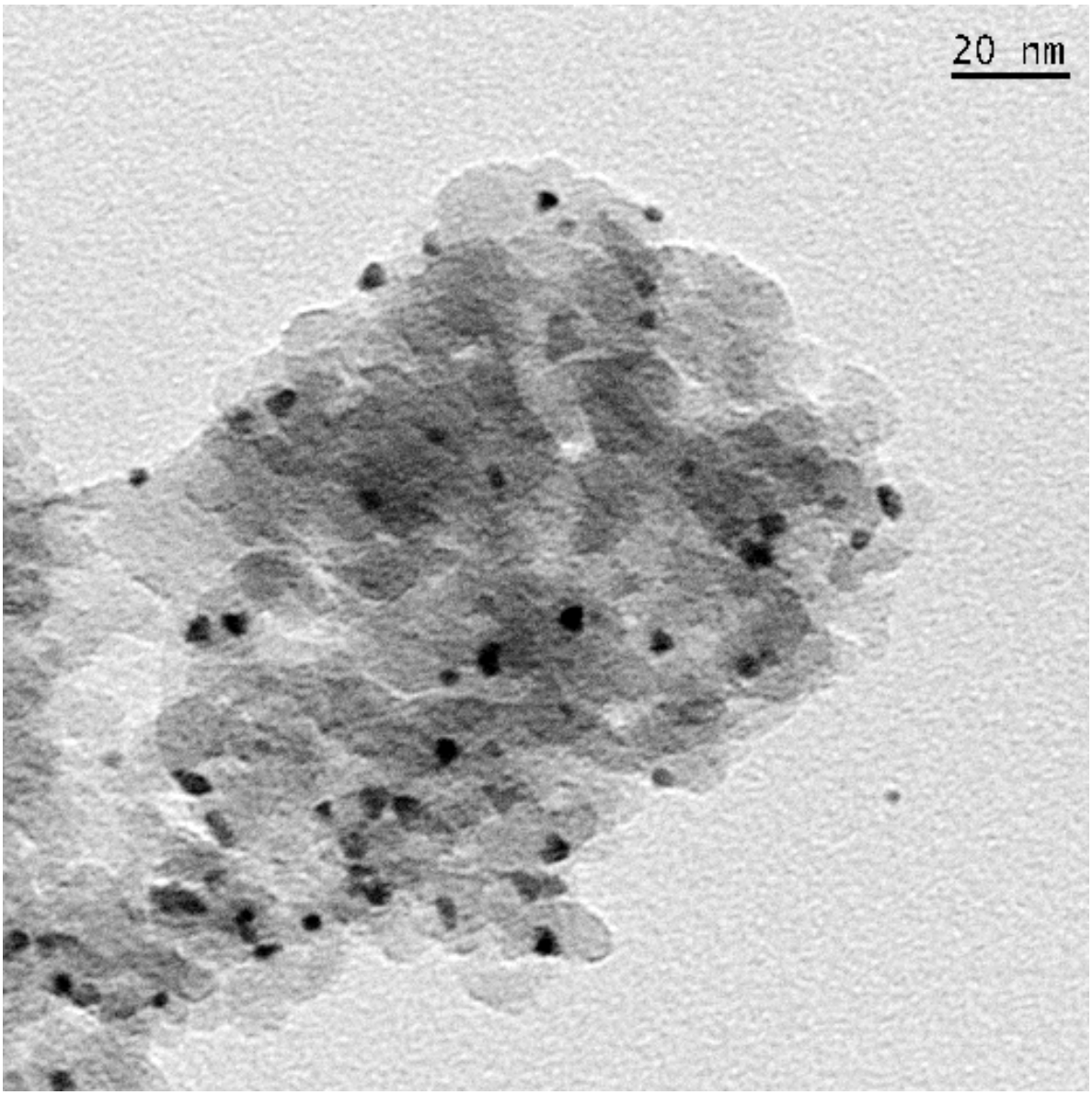

Figure 3.10 TEM image of 0.5 wt% supported tetrahedral Pt/SiO_2 prepared by Dr. Ilkeun Lee

Table 3.1 shows the results from the experiments with various catalysts. Depending on the catalyst, different conversion and product distribution were observed. In terms of conversion, catalysts with larger particle size resulted in slower reaction, which is likely to be due to small surface area. Tetrahedral catalyst resulted in much slower reaction compared to normal catalysts possibly due to low particle dispersion or the capping agent and organic residues.

The main product on all four catalysts was butylaldehyde produced via C=C hydrogenation. Also, some hydrocarbons, such as propylene were observed. These products should have been resulted from decarbonylation. The desired product, crotylalcohol, however, could not be obtained with any of the catalysts employed in this study. Therefore no meaningful results about the effect of particle size or particle shape could obtain in this set of experiments.

3.3.2. Other hydrogenation reactions

Hydrogenation was also carried out with various reactants that have more than two potential hydrogenation products. Acrolein, methyl vinyl ketone, acrylonitrile styrene, furan, pyrrole, acrylonitrile, pyruvonitrile, and 2-methylfuran were all tested at various temperatures with normal catalysts. However no more than two main products was obtained. Therefore none of the reaction seems to be a good test reaction to investigate the effect of shape controlled catalysts on the product distribution.

Table 3.1. Hydrogenation of crotonaldehyde on normal- and tetra-Pt/SiO_2

Catalyst	Ox temp	Conversion	HC	BUAL	BUOL	CROL	Others
Normal-Pt	300	41.7	21.8	75.7	0.7	0.0	1.8
Normal-Pt	500	36.3	20.1	73.3	1.0	0.0	5.6
Normal-Pt	700	29.3	12.3	83.6	0.9	0.0	3.2
Tetra-Pt	-	5.9	15.9	77.2	0.0	0.0	6.9

CRAL: 10 Torr, H_2: 100 Torr, Ar: 490 Torr

HC: hydrocarbons, BUAL: buthylaldehyde, BUOL: buthylalcohol, CROL: crothylalcohol

Others: acetaldehyde, acetone, propionaldehyde, etc

3.3.3. Hydrogenation of isoprene

3.3.3.1. Preliminary results

Preliminary study was conducted with 0.5 wt% normal Pt/SiO_2 calcined at 500 °C (Fig. 3.7) and the same 0.5 wt% tetrahedral Pt/SiO_2 catalyst used in crotonaldehyde hydrogenation made by Dr. Ilkeun Lee (Fig. 3.10). The reaction was carried out with both coarse and silanized wool. Normal catalyst was reduced at 300 °C for 1 h and tetrahedral catalyst was reduced at 200 °C for 1 h to avoid potential deformation of the catalyst particles.

Fig. 3.11 shows the obtained products on normal and tetrahedral catalysts. Quite different product distribution was obtained on two catalysts. In addition, the product distribution on tetrahedral catalyst was very similar to that on Pt(111) reported by Vassilakis[9]. Therefore it was expected that different particle shape, thus different exposed facet resulted in different product distribution.

These results were very promising. However, they could not be reproduced when the experiments were repeated. Reaction rate varied widely. The product distribution on normal catalyst became similar to that on tetrahedral catalyst, although it was not quite reproducible either.

3.3.3.2. Reproducibility improvement

In order to improve reproducibility, investigation was conducted to identify the possible sources that affect the reaction. The possible sources that were considered are: backstreaming of

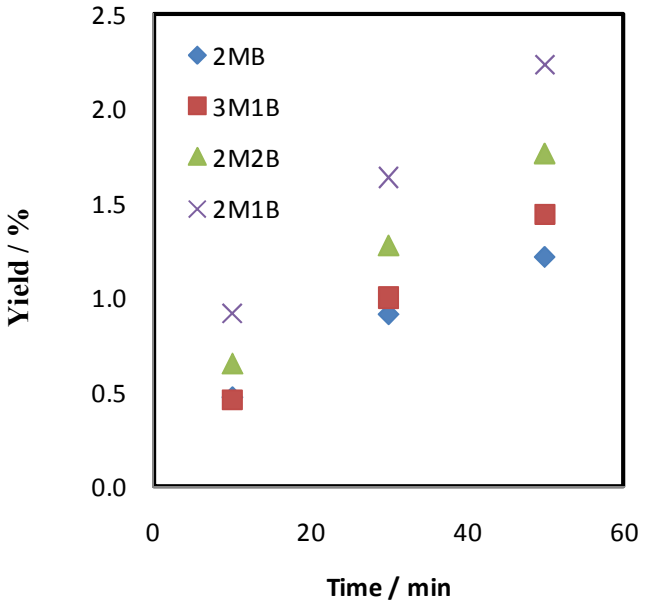

0.5 wt% normal Pt/SiO_2

(calcined at 500 °C)

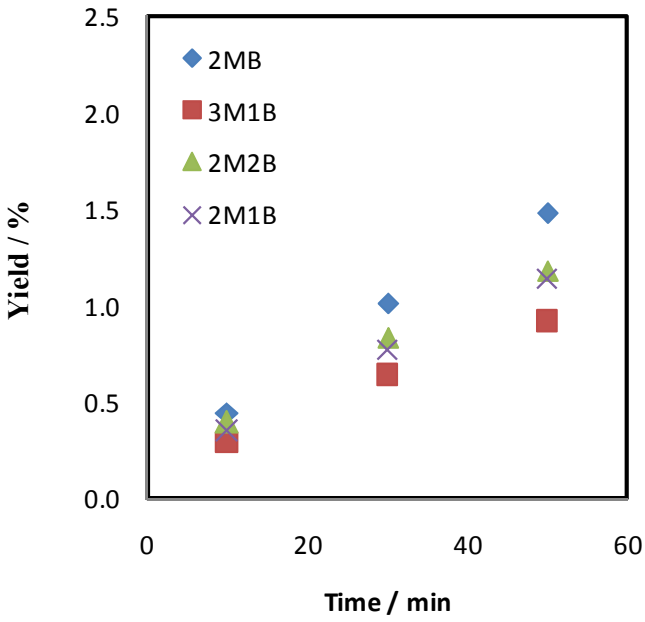

0.5 wt% tetrahedral Pt/SiO_2

(Prepared by Dr. Ilkeun Lee)

Fig. 3.11 Isoprene hydrogenation on 0.5 wt% normal and tetrahedral Pt/SiO_2 (preliminary result)

oil from vacuum pump, poor circulation/mixing of gases, impurities in isoprene, impurities in hydrogen, impurities in argon, insufficient catalyst activation, and contamination of the reactor. In order to eliminate these possible sources, various test experiments were conducted: installation of liquid nitrogen trap between the reactor and the pump, circulation test with ethylene and propylene, use of new batch of isoprene, use of ultra-high purity gases, CO adsorption test in infrared system after reduction at various temperatures, and cleaning of the reactor. It seemed like that none of these possible sources are affecting the reaction. Use of liquid nitrogen trap, new batch of isoprene, and ultra-high purity gases did not make any difference in reaction. It was confirmed that gases get fully mixed by the circulation pump. Also, it was confirmed that normal catalyst gets fully reduced after reduction as low as 150 °C.

Accidentally, it was found that much faster reaction rate could be obtained when silanized wool was not used. Fig 3.12 shows the comparison between the reaction results when both coarse and silanized wool were used and that when only silanized wool was used. 1.0 wt% Normal Pt catalyst was used. Much faster reaction was observed when silanized wool was not used. Silanized wool should be very inert and should not affect catalytic reaction, but it changed the result dramatically. Also, much better reproducibility in both reaction rate and selectivity was obtained without silanized wool.

3.3.3.3. Reaction without silanized wool and coarse wool

Although the reproducibility improved by using only coarse wool, it was found that reduction treatment significantly decreases the reaction rate. Fig. 3.13 shows obtained reaction results after no treatment (only evacuation), reduction at 300 °C for 1h, and oxidation at 300 °C for 1h. 5 mg of 0.2 wt% normal catalyst was used because the reaction rate became much faster by not using

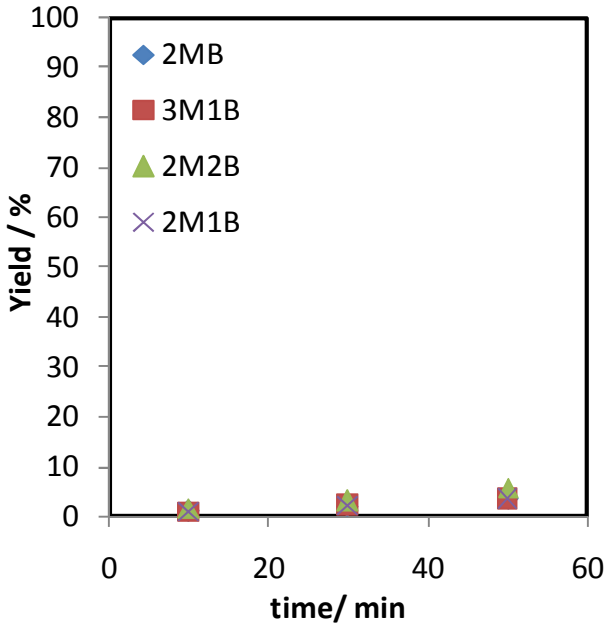

With silanized wool

1.0 wt% normal Pt/SiO_2

(calcined at 300 °C)

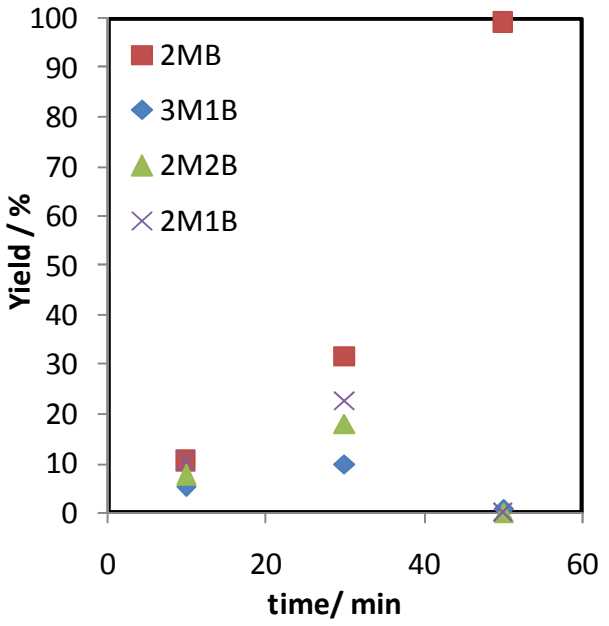

Without silanized wool

1.0 wt% normal Pt/SiO_2

(calcined at 300 °C)

Fig. 3.12 Isoprene hydrogenation on normal Pt/SiO_2 with or without silanized wool

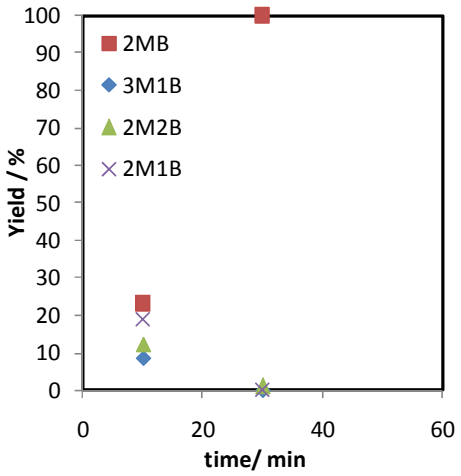

After evacuation (no treatment)

0.2 wt% normal Pt/SiO_2

(calcined at 300 °C)

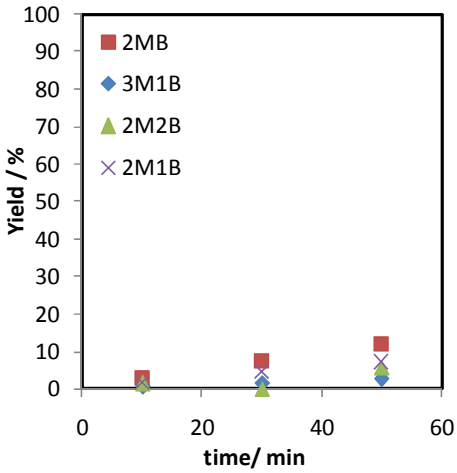

After reduction at 300 °C for 1h

0.2 wt% normal Pt/SiO_2

(calcined at 300 °C)

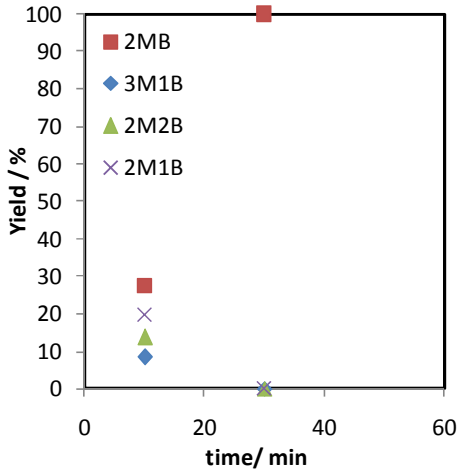

After oxidation at 300 °C for 1h

0.2 wt% normal Pt/SiO_2

(calcined at 300 °C)

Fig. 3.13 Isoprene hydrogenation - effect of pretreatment with coarse wool

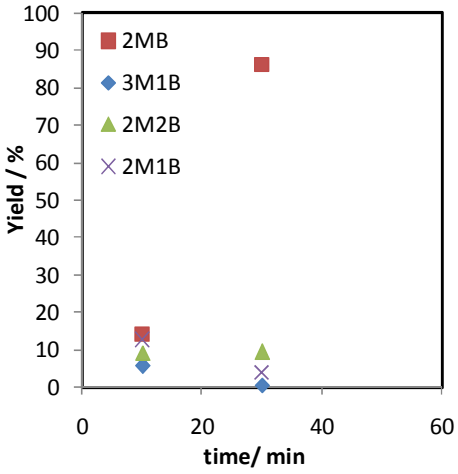

After evacuation (no treatment)

0.2 wt% normal Pt/SiO_2

(calcined at 300 °C)

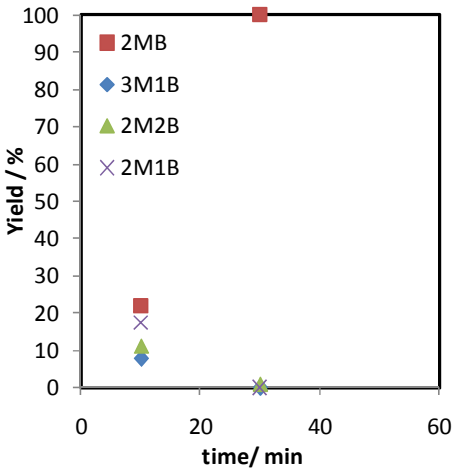

After reduction at 300 °C for 1h

0.2 wt% normal Pt/SiO_2

(calcined at 300 °C)

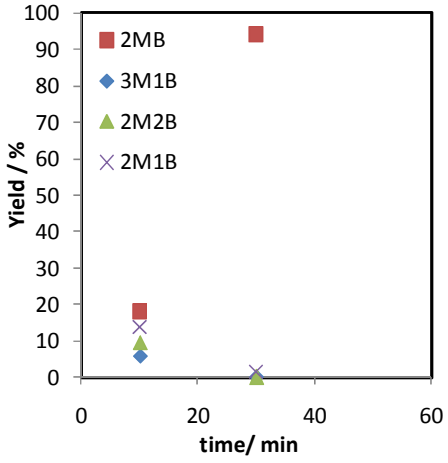

After oxidation at 300 °C for 1h

0.2 wt% normal Pt/SiO_2

(calcined at 300 °C)

Fig. 3.14 Isoprene hydrogenation – effect of pretreatment without coarse wool

silanized wool. Much slower reaction was observed after reduction of the catalyst. This suggests that the reaction is faster when the catalyst surface is oxidized, or catalyst gets deactivated somehow during reduction treatment. It is highly unlikely because it is very well known that Pt catalysts are the most active when it is reduced into metallic Pt^0 state. Some sort of contaminants can be present in the reactant and deactivates the catalyst during reduction treatment.

The same set of experiments was conducted in another circulation reactor in our research group. Using 5mg of 0.2 wt% of Pt/SiO_2 with coarse wool. Slow reaction after reduction was also observed. This suggests that it is unlikely that some contaminants in the reactor were causing this slow reaction after reduction. This reactor was used for cis-trans isomerization of butanes, therefore this phenomenon could have also occurred in cis-trans isomerization experiments.

Also, using propylene as reactant, it was tested if the same phenomenon by reduction would occur. Slow reaction was indeed observed in propylene hydrogenation after reduction of catalyst. Therefore this phenomenon is not particular to hydrogenation of isoprene.

Also, the reaction without either silanized wool or coarse wool was conducted. The catalyst was directly placed on the bottom of the glass u-tube. Evacuation and introduction of gases were carefully done not to blow away catalyst power. As shown in Fig. 3.14, almost the same reaction rate was observed after reduction without coarse wool. Therefore it is likely that this coarse wool was causing the slow reaction after reduction treatment, although this behavior is very strange since wool should not affect the catalytic activity. However it seemed that it is best to compare the catalytic activities of different catalysts without using any wool.

3.3.3.4 Preparation of tetrahedral catalyst

Supported tetrahedral catalyst provided from Dr. Ilkeun Lee did not seem to have much defined tetrahedral particles, therefore preparation of tetrahedral catalysts was conducted.

Basically the same method was used as what Dr. Ilkeun Lee did. The preparation was repeated slightly changing the condition such as bubbling speed of hydrogen, batch of PVP solution, batch of milli-Q water, batch of H_2PtCl_6 solution, and container for preparation. Gas bubbling was conducted using a stainless steel tube, but there was a possibility that H_2PtCl_6 reacts with the metal surface so the preparation was also conducted using a glass tube for gas bubbling. Despite this effort to optimize the preparation condition, defined tetrahedral Pt particles could not be obtained reproducibly. Fig. 3.15 shows TEM images of two samples that have relatively defined tetrahedral particles and that have poor shape. These two samples were prepared in the same condition. I could not produce particularly better sample compared to the one provided from Dr. Ilkuen Lee (Fig. 3.8).

One of the best samples with relatively defined tetrahedral particles was deposited on SiO_2 xerogel provided from Dr. Ilkeun Lee. Fig. 3.16 shows TEM images of supported tetrahedral particles. Some particles seem to still have relatively defined tetrahedral shape after deposition.

3.3.3.5. Preparation of cubic catalyst

Preparation of cubic Pt catalyst was also conducted. This was also done by the same method as Dr. Ilkeun Lee did in the past. The preparation was repeated slightly changing the condition such as batch of K_2PtCl_4 solution, batch of SPA solution, and amount of SPA solution (0.5, 0.75, 1.0

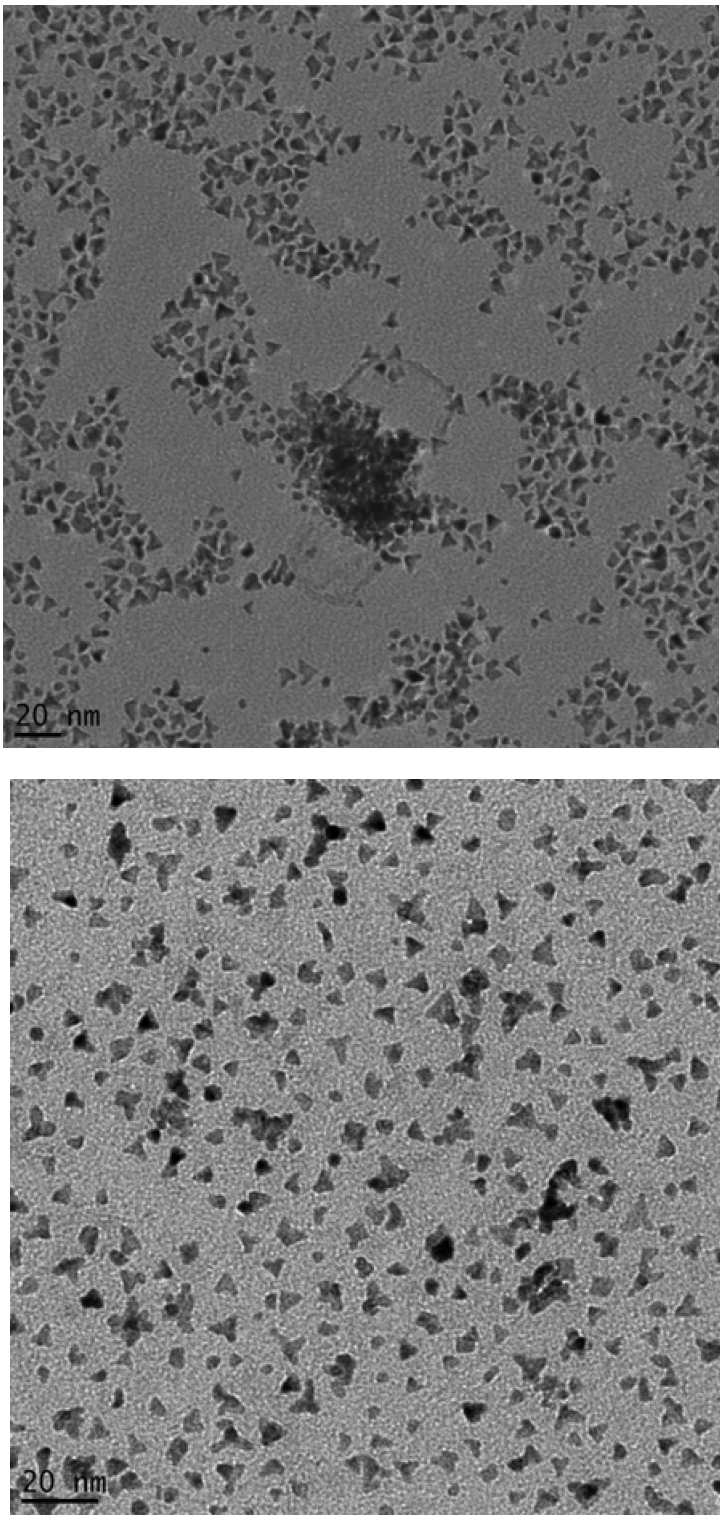

Figure 3.15 Colloidal tetrahedral particles

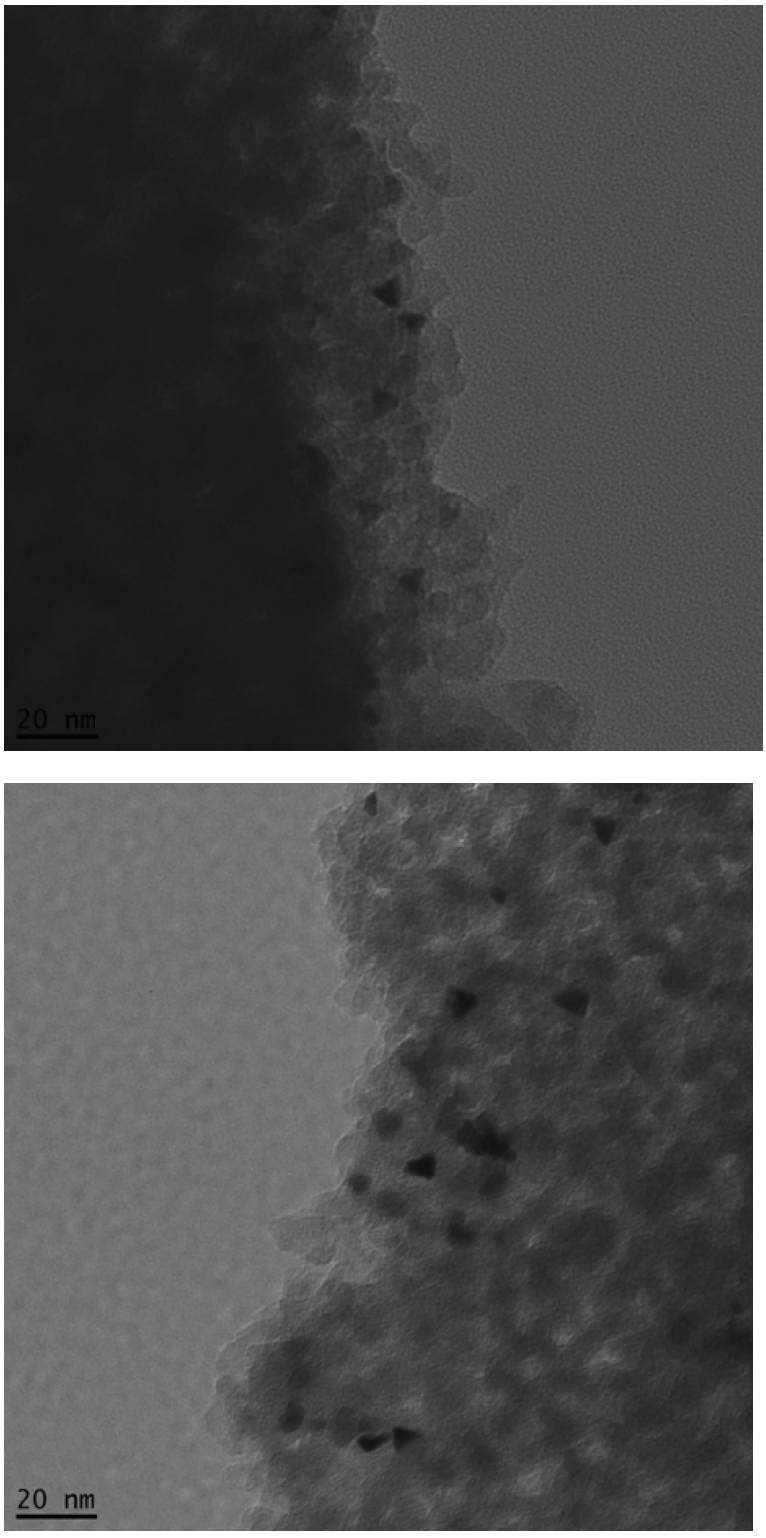

Figure 3.16 0.5 wt% supported tetrahedral particles

ml), bubbling speed. Fig. 3.17 shows TEM pictures of the sample with the most defined particle shape. Some particles may have cubic shape, although not very defined. Many particles seem to have more like cuboctahedral shape. This sample was also deposited on the same xerogel SiO_2.

Fig. 3.18 shows TEM images of cubic Pt/SiO_2. Most of cubic particles seem to be aggregated, although the shape of particles still looked almost the same as that before deposition. The particles seem to be tangled with polymer and that inhibited the dispersion.

3.3.3.6. Comparison of catalysts

Finally, activity test of obtained catalysts were conducted. 0.5 wt% normal Pt/SiO_2 (calcinated at 500 °C), 0.5 wt% tetrahedral Pt/SiO_2, and 0.5 wt% cubic Pt/SiO_2 were employed. The reaction was conducted after 1) no treatment, 2) reduction at 300 °C, and 3) oxidation at 300 °C. The catalysts were placed directly in the u-tube without using wool. The results are shown in Fig. 3.20-3.21.

First of all, neither particle shape nor pretreatment condition affected the product distribution. The order to selectivity into each product was always 2MB, 2M1B, 2M2B, then 3M1B. Therefore, no effect of particle shape on selectivity could be observed.

In terms of catalytic activity, it can be said that normal Pt/SiO_2 was more active than tetrahedral and cubic Pt/SiO_2. This seems to be due to either poorer dispersion of Pt particles or surfactant polymer on the catalyst particles. However the catalytic activity of tetrahedral and

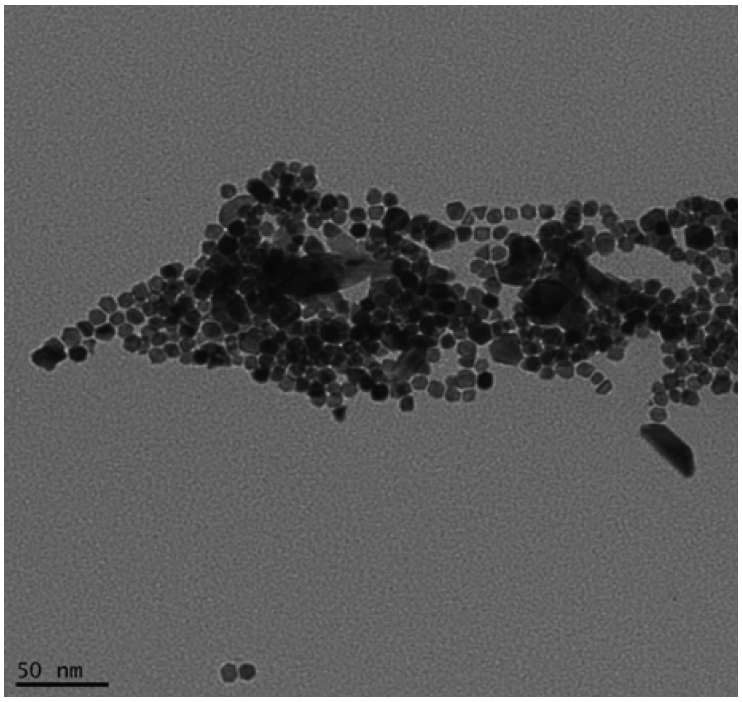

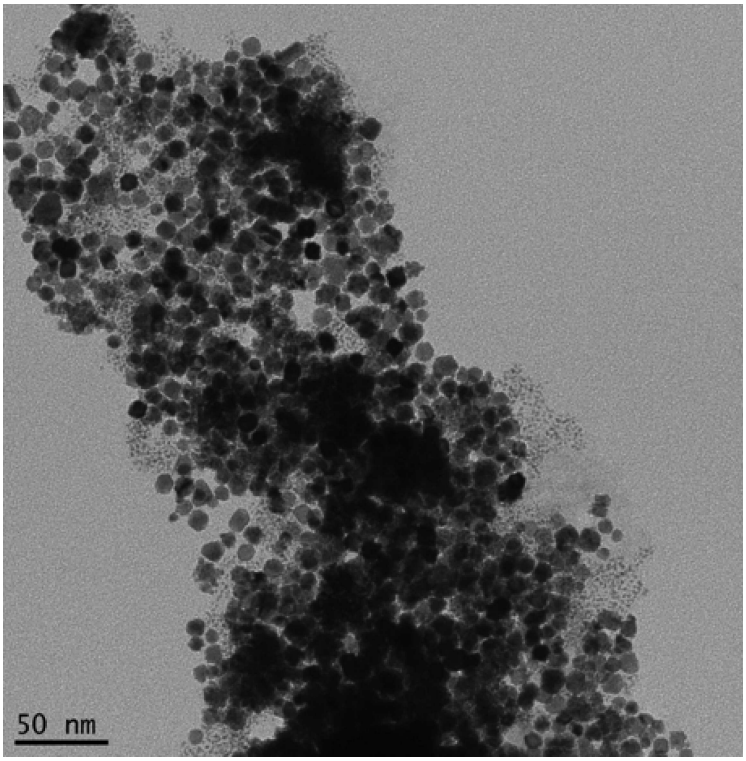

Figure 3.17 colloidal cubic particles

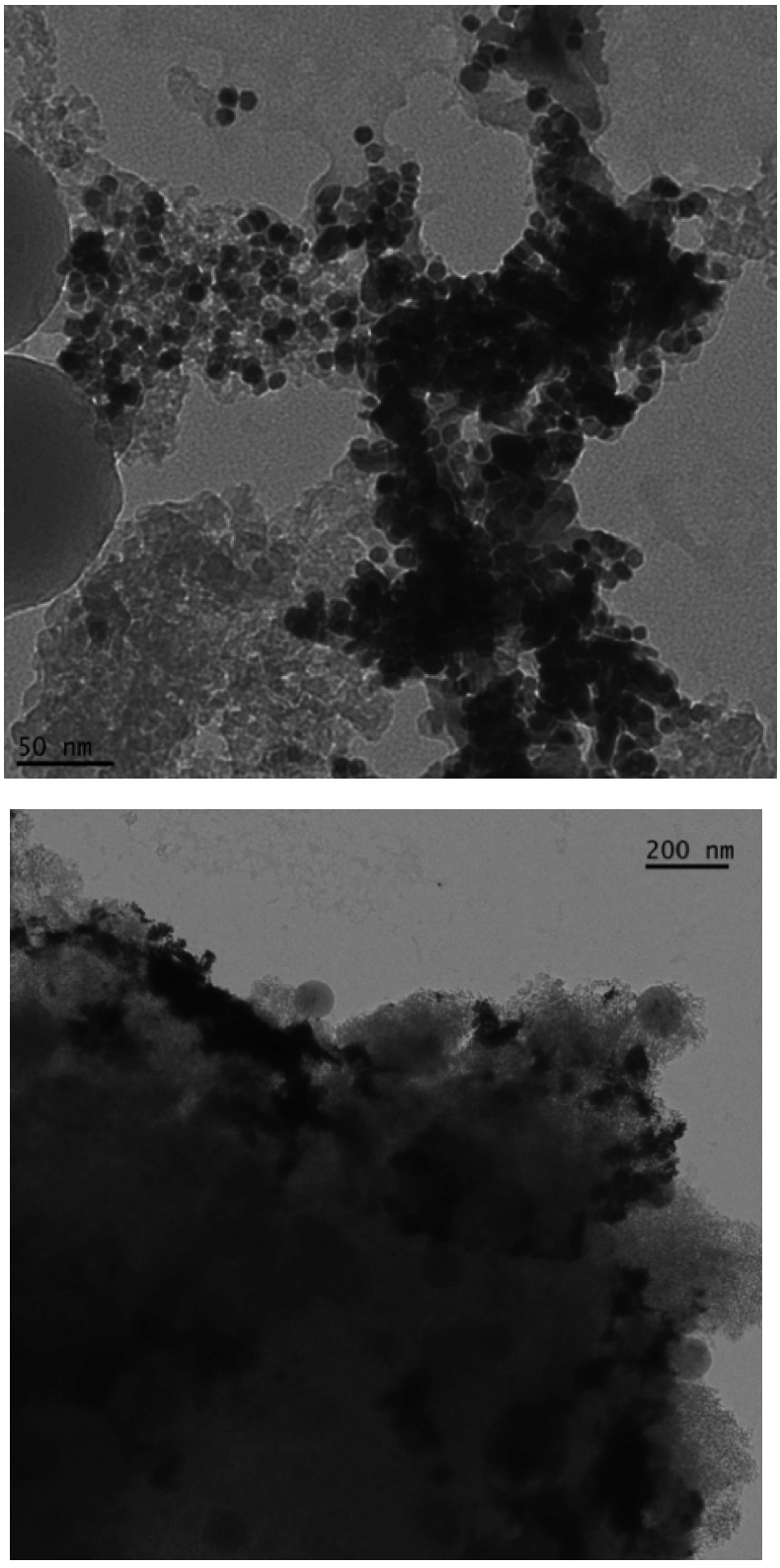

Figure 3.18 0.5 wt% supported cubic particles

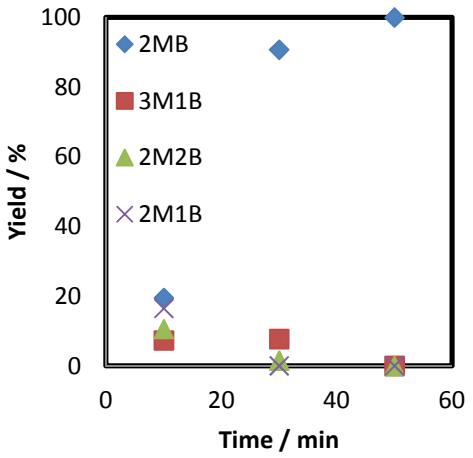

After evacuation (no treatment)

0.5 wt% normal Pt/SiO_2

(calcined at 500 °C)

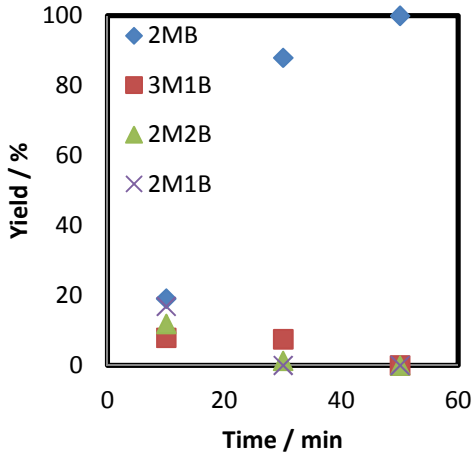

After reduction at 300 °C for 1h

0.5 wt% normal Pt/SiO_2

(calcined at 500 °C)

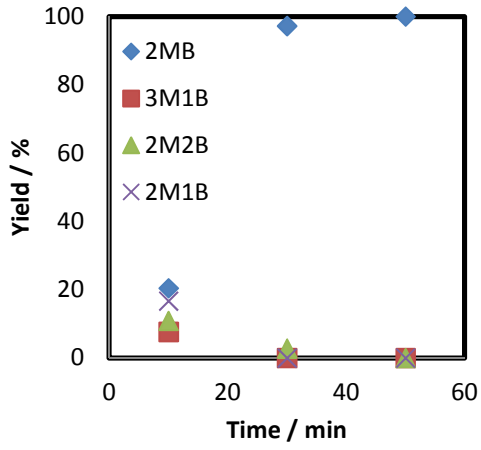

After oxidation at 300 °C for 1h

0.5 wt% normal Pt/SiO_2

(calcined at 500 °C)

Figure 3.19 Hydrogenation of isoprene on 0.5 wt% normal Pt/SiO_2

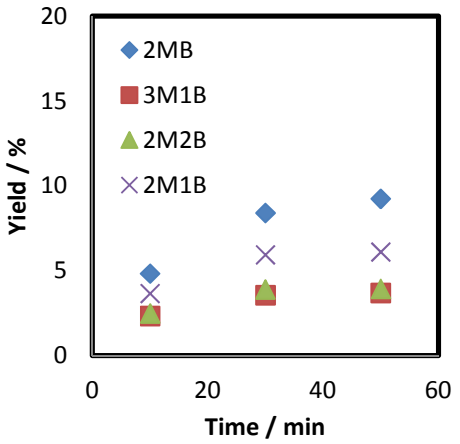

After evacuation (no treatment)

0.5 wt% tetrahedral Pt/SiO_2

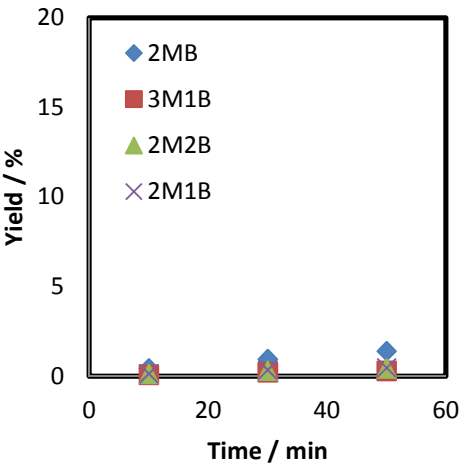

After reduction at 300 °C for 1h

0.5 wt% tetrahedral Pt/SiO_2

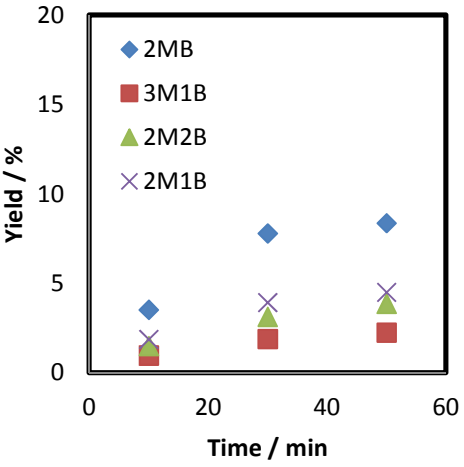

After oxidation at 300 °C for 1h

0.5 wt% tetrahedral Pt/SiO_2

Figure 3.20 Hydrogenation of isoprene on tetrahedral Pt/SiO_2

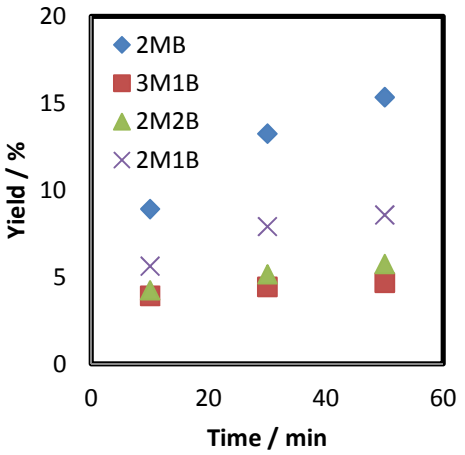

After evacuation (no treatment)

0.5 wt% cubic Pt/SiO_2

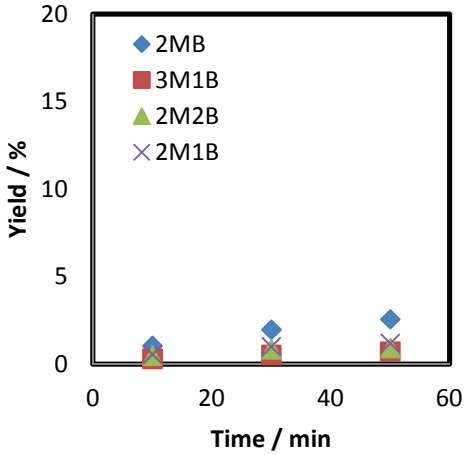

After reduction at 300 °C for 1h

0.5 wt% cubic Pt/SiO_2

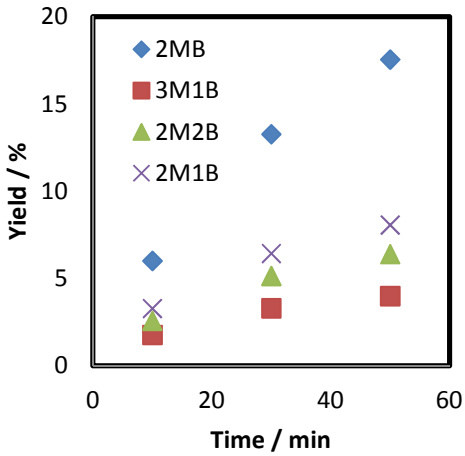

After oxidation at 300 °C for 1h

0.5 wt% cubic Pt/SiO_2

Figure 3.21 Hydrogenation of isoprene on cubic Pt/SiO_2

about trans-cis isomerization of butenes, surfactants can be removed by calcination at well below 300 °C. This seems to mean that the supported colloidal catalysts are fully functional even when the surfactants still exist, although it is hard to believe.

Reaction on tetrahedral and cubic Pt/SiO_2 seemed to slow down during the reaction when no treatment was done (see the top figures in 3.20 and 3.21). Also, on tetrahedral and cubic catalysts, slower reaction was observed after reduction. Possibly the surfactants may have caused these deactivation of the catalyst somehow.

3.4. Conclusions

Hydrogenation of isoprene, crotonaldehyde, and various other reactants were conducted to see if any effect of particle shape could be seen on product selectivity in hydrogenation in which two or more possible products can be obtained. Only in hydrogenation of isoprene, two or more products could actually be obtained.

It was suggested that coarse and silanized wools were causing some unwanted effects on the catalyst, therefore catalytic activity test was conducted by placing the catalyst on the bottom of the glass u-tube.

Preparation of tetrahedral and cubic catalysts was conducted repeatedly slightly changing the preparation condition. Obtained cubic samples did not contain much cubic particles. Also, cubic particles seem to aggregate upon deposition on SiO_2 xerogel.

No difference in product distribution was observed among normal, tetrahedral, and cubic catalysts. Tetrahedral and cubic particles had almost the same catalytic activity before any treatment and after oxidation at 300 °C, which seem to mean that colloidal catalysts are active without a removal of surfactant molecules. Slower reaction was observed after reduction on tetrahedral and cubic catalysts.

References

(1) Taylor, H. In *Proceedings of the Royal Society of London Series A*; 1925; Vol. 108, pp. 105–111.
(2) Sinfelt, J. *Advances in Catalysis*; Advances in Catalysis; Elsevier, 1973; Vol. 23, pp. 91–119.
(3) Ertl, G. *Catalysis Reviews* **1980**, *21*, 201–223.
(4) Somorjai, G. A.; Materer, N. *Top Catal* **1994**, *1*, 215–231.
(5) Lee, I.; Zaera, F. *J. Am. Chem. Soc.* **2005**, *127*, 12174–12175.
(6) Lee, I.; Zaera, F. *Journal of Catalysis* **2010**, *269*, 359–366.
(7) Lee, I.; Morales, R.; Albiter, M. A.; Zaera, F. *Proceedings of the National Academy of Sciences* **2008**, *105*, 15241–15246.
(8) Lee, I.; Delbecq, F.; Morales, R.; Albiter, M. A.; Zaera, F. *Nature Materials* **2009**, *8*, 132–138.
(9) Vassilakis, D.; Margot, E.; Pradier, C. M.; Berthier, Y. *Journal of Molecular Catalysis* **1990**, *61*, 41–50.
(10) Grass, M. E.; Rioux, R. M.; Somorjai, G. A. *Catal Lett* **2008**, *128*, 1–8.
(11) Vannice, M. *Journal of Catalysis* **1989**, *115*, 65–78.
(12) Abid, M.; Paul-Boncour, V.; Touroude, R. *Applied Catalysis A: General* **2006**, *297*, 48–59.

Chapter 4: Conclusions

In chapter 2, adsorption of (S)- and (R)-PO on (R)-NEA covered Pt(111) surface was described. Contrary to reported experiments with (S)-NEA, only one monolayer peak of PO was observed. Also desorption temperatures of (R)-PO and (S)-PO were essentially the same. These two facts strongly suggest that there is no strong 1:1 interaction between (R)-NEA and (R)-PO. It would be very strange if a 1:1 complex formation only occurs with SS pair but not with RR pair. No sharp drop between monolayer and multilayer desorption peak was observed, and a clear gradual shift from monolayer peak to multilayer peak was observed as (R)-NEA exposure was increased. Slight enantioselective enhancement of (R)-PO adsorption compared to (S)-PO when the surface is partially covered (~1 L) was observed both in RAIRS and TPD, suggesting templating model of (R)-NEA.

In chapter 3, hydrogenation of isoprene, crotonaldehyde, and various other reactants were summarized. Only in hydrogenation of isoprene, two or more products could actually be obtained. It was suggested that coarse and silanized wools were causing some unwanted effects on the catalyst, therefore catalytic activity test was conducted by placing the catalyst on the bottom of the glass u-tube. Preparation of tetrahedral and cubic catalysts was conducted repeatedly slightly changing the preparation condition. Obtained cubic samples did not contain much cubic particles. Also, cubic particles seem to aggregate upon deposition on SiO_2 xerogel. No difference in product distribution was observed among normal, tetrahedral, and cubic catalysts in isoprene hydrogenation. Tetrahedral and cubic particles had almost the same catalytic activity before any treatment and after oxidation at 300 °C, which seem to mean that colloidal catalysts are active

without a removal of surfactant molecules. Slower reaction was observed after reduction on tetrahedral and cubic catalysts.